The Astrophysical Journal, 1003:46 (15pp), 2026 May 20 https://doi.org/10.3847/1538-4357/ae610f

SDSS J110546.07+145202.4: The First Long-duration Radio Changing-look NLS1 Galaxy

S. Komossa[1], D. Grupe[2], A. Kraus[1], P.G. Edwards[3], E. F. Kerrison[3,4], K. Rose[4,3], R. Soria[5,4], T. An[6,7], M.J. Hardcastle[8], K.É. Gabányi[9,10,11,12], S. Panda[13,16], D.W. Xu[14,15], J. Wang[14], S. Frey[11,12], and A. Mezősi[9]
[1] Max-Planck-Institut für Radioastronomie, Auf dem Hügel 69, 53121 Bonn, Germany; skomossa@mpifr.de
[2] Department of Physics, Geology, and Engineering Technology, Northern Kentucky University, Nunn Drive, Highland Heights, KY 41099, USA
[3] CSIRO Space and Astronomy, Australia Telescope National Facility, PO Box 76, Epping, NSW 1710, Australia
[4] Sydney Institute for Astronomy, School of Physics, The University of Sydney, NSW 2006, Australia
[5] INAF-Osservatorio Astrofisico di Torino, Strada Osservatorio 20, I-10025 Pino Torinese, Italy
[6] State Key Laboratory of Radio Astronomy and Technology, Shanghai Astronomical Observatory, Chinese Academy of Sciences, 80 Nandan Road, Shanghai 200030, People's Republic of China
[7] Department of Astronomy, University of Science and Technology of China, Hefei, Anhui 230026, China
[8] Department of Physics, Astronomy and Mathematics, University of Hertfordshire, College Lane, Hatfield AL10 9AB, UK
[9] Department of Astronomy, Institute of Physics and Astronomy, ELTE Eötvös Loránd University, Pázmány Péter sétány 1/A, 1117 Budapest, Hungary
[10] HUN-REN–ELTE Extragalactic Astrophysics Research Group, ELTE Eötvös Loránd University, Pázmány Péter sétány 1/A, 1117 Budapest, Hungary
[11] Konkoly Observatory, HUN-REN Research Centre for Astronomy and Earth Sciences, Konkoly-Thege Miklós út 15-17, 1121 Budapest, Hungary
[12] CSFK, MTA Centre of Excellence, Konkoly-Thege Miklós út 15-17, 1121 Budapest, Hungary
[13] International Gemini Observatory/NSF NOIRLab, Casilla 603, La Serena, Chile
[14] Key Laboratory of Space Astronomy and Technology, National Astronomical Observatories, Chinese Academy of Sciences, Beijing 100101, People's Republic of China
[15] School of Astronomy and Space Science, University of Chinese Academy of Sciences, Beijing, People's Republic of China
Received 2026 January 23; revised 2026 April 14; accepted 2026 April 15; published 2026 May 13

Abstract

SDSS J110546.07+145202.4 stands out as a unique radio changing-look narrow-line Seyfert 1 (NLS1) galaxy that has brightened dramatically and shows an exceptionally long duration of its "on" phase. We present the first high-frequency radio observations, the first simultaneous radio spectral energy distributions (SEDs), the first optical/UV/X-ray SEDs, and the first X-ray monitoring and spectroscopy of this recently discovered event. Importantly for understanding the nature of the outburst, we show that the X-ray spectrum is soft with a photon index of $\Gamma_X = 2.5$; line-of-sight absorption and extinction are low or absent; the radio SED is peaked at low frequencies of ~2 GHz; and the radio outburst emission is very long-lived ($t > 8$ yr) and roughly constant. The softness of the X-ray spectrum, low supermassive black hole (SMBH) mass, and high Eddington ratio all corroborate the optical NLS1 classification. We discuss multiple outburst scenarios, including lensing, absorption, a binary SMBH merger, a long-duration giant-star tidal disruption, a newly ignited active galactic nucleus, and an accretion-rate change. While most of them can be either excluded or are deemed too rare and lack positive evidence so far, most or all types of these transients are expected to be detected in ongoing Very Large Array and upcoming Square Kilometre Array surveys. SDSS J110546.07+145202.4 itself is well explained by an accretion rate change that triggered the powerful radio jet emission. The low redshift and SMBH mass of this system offer a unique perspective into the physical processes of radio-jet ignition that are expected to have operated in the early Universe around growing SMBHs.

Unified Astronomy Thesaurus concepts: Extragalactic radio sources (508); Radio transient sources (2008); Radio active galactic nuclei (2134); X-ray active galactic nuclei (2035); Active galactic nuclei (16)

1. Introduction

Astrophysical transients shed new light on physics in extreme environments, often in the vicinity of (super)massive black holes. In the radio regime, transients probe the early formation and evolution of jets and outflows, and/or the physics of accretion disk - corona systems, in a regime that is typically different from classical blazars or Galactic binaries, and at short timescales that can be observed conveniently. Long-lived extragalactic radio transients on timescales of weeks to years include the afterglows of gamma-ray bursts (D. A. Frail et al. 1997; P. J. Hancock et al. 2013), radio supernovae (S. Sukumar & R. J. Allen 1989; M. F. Bietenholz et al. 2021; K. Rose et al. 2024), stellar tidal disruption events (TDEs; J. S. Bloom et al. 2011; A. Anumarlapudi et al. 2024; D. Li et al. 2025), different forms of unusual active galactic nuclei (AGN) outbursts (J. Y. Koay et al. 2016; K. Nyland et al. 2020; M. Kunert-Bajraszewska et al. 2020; A. Wołowska et al. 2021; S. Birmingham et al. 2025; E. T. Meyer et al. 2025), and as yet unidentified transients from the centers of galaxies (F. Zhang et al. 2022; M. Kunert-Bajraszewska et al. 2025; Y. Chen et al. 2025). Past and ongoing radio surveys represent excellent databases to search for such transient events on timescales of months to decades.

Narrow-line Seyfert 1 (NLS1) galaxies and their higher-luminosity counterparts, NL type 1 quasars (NLQ1s hereafter),[17] are a subgroup of AGN that are of great interest due to

[16] Gemini Science Fellow.

[17] As is common in the literature, we collectively refer to them as NLS1 galaxies, except if noted otherwise.

their location at one extreme end of AGN correlation space (J. W. Sulentic et al. 2000; T. A. Boroson 2002; D. Grupe 2004; D. Xu et al. 2012; P. Marziani et al. 2018). They host low-mass black holes that, on average, accrete close to the Eddington limit. They therefore represent important local cases (see the review by S. Komossa 2008) to study the physics of the rapid supermassive black hole (SMBH) growth expected to have operated in the early Universe, which JWST is now witnessing (R. Maiolino et al. 2024). In the radio regime, NLQ1s and NLS1s have been found to be less frequently radio-loud than their broad-line counterparts (broad-line Seyfert 1s and broad-line type 1 quasars; BLS1s and BLQ1s, hereafter). Only ∼7% of NLQ1s are radio-loud (S. Komossa et al. 2006; S. Rakshit et al. 2017; S. Chen et al. 2022), and only 2.5% are very radio-loud (S. Komossa et al. 2006). Nevertheless, like their broad-line counterparts, a small fraction of NLS1s and NLQ1s host relativistic jets and show multiwavelength (MWL) properties similar to those of blazars (H. Zhou et al. 2007; W. Yuan et al. 2008; S. Komossa 2018; M. Lister 2018), extending the blazar regime to lower SMBH masses (Figure 4 of S. Komossa et al. 2006) than found in classical blazars and radio-loud quasars. Radio variability of NLS1 galaxies as a class is relatively rare; typically much less than a factor of 2 and up to ∼5 in rare cases with relativistic jets and at high frequencies $\gtrsim$5 GHz (W. Yuan et al. 2008; E. Angelakis et al. 2015; X. Shao et al. 2025).

Radio properties of NLS1 galaxies in general, and high-amplitude radio outbursts in particular, provide us with important insights into the physics of the jet-disk symbiosis, particle acceleration, jet–gas interaction in gas-rich and dense circumnuclear environments different from classical blazars, and feedback processes potentially relevant for galaxy evolution.

Here, we report follow-up observations and interpretation of the long-lasting, high-amplitude radio outburst of the nearby NLS1 galaxy SDSS J110546.07+145202.4 (hereafter SDSS J1105+1452) reported by K. É. Gabányi et al. (2025, hereafter GKK25) with an amplitude of a factor >23 at 1.4 GHz.

The MWL properties of SDSS J1105+1452 have been little studied in depth before. Its optical spectrum, obtained in the course of the Sloan Digital Sky Survey (SDSS; D. G. York et al. 2000) and included in a number of SDSS large-sample studies (e.g., K. Oh et al. 2015; J. Sun & Y. Shen 2015; S. Rakshit et al. 2017; V. S. Paliya et al. 2024), is that of an NLS1 galaxy at redshift $z = 0.1209$. It shows FWHM(H$\beta_{\rm broad}$) $=1498\ {\rm km\ s^{-1}}$ (J. Sun & Y. Shen 2015), strong Fe II emission complexes (R4570=0.92, S. Rakshit et al. 2017), and [O III] 5007/Hβ < 3, and therefore fulfills all NLS1 classification criteria.[18] SDSS J1105+1452 was detected in X-rays in the ROSAT all-sky survey (RASS; W. Voges et al. 1999). Based on its absolute B-band magnitude of $M_{\rm B} = -20.7$ (V. S. Paliya et al. 2024), it is in the Seyfert (not the quasar) regime. It was identified as radio-emitting NLS1 (S. Rakshit et al. 2017) and detected by LOFAR (I. Varglund et al. 2025). SDSS J1105+1452 was radio faint (near the detection limit) in the Faint Images of the Radio Sky at Twenty centimeters (FIRST; R. L. White et al. 1997) survey, but has brightened by a factor of ∼20 since 2017.96 and has turned radio-loud (GKK25). We introduce the term "radio changing-look" to refer to high-amplitude radio variability, especially leading to a change between radio-quiet and radio-loud, or vice versa. This is in analogy to the term X-ray changing-look (G. Matt et al. 2003), which refers to high-amplitude absorption changes in X-rays, and optical changing-look (S. M. LaMassa et al. 2015), which refers to high-amplitude broad-line and/or continuum variability.

Such radio variability has rarely been observed so far. Among the population of BLQ1s, a few have shown remarkable, strong brightening in the radio band and transitioned to radio-loud (M. Kunert-Bajraszewska et al. 2020; K. Nyland et al. 2020), none as long-lived as SDSS J1105+1452, and none in a low-mass AGN or NLS1 galaxy in particular. A few NLS1s exhibit giant-amplitude radio flaring (E. Järvelä et al. 2024), but these turn on and off on timescales as short as hours to days, primarily seen at high frequencies (37 GHz), and deep high-resolution imaging did not show evidence for long-lived jets in the majority of these systems.

To understand the physics behind the long-lived radio changing-look event of SDSS J1105+1452, we have obtained multiple new MWL observations, many of them for the first time. This paper is organized as follows. In Section 2, we present the Swift X-ray observations. Section 3 reports Swift UV-optical observations. In Section 4, new radio observations acquired with the Effelsberg 100 m telescope and ATCA are presented along with new archival radio observations. Section 5 gives a summary of archival IR and optical observations dating back to 2003 and in one case to the 1950s. These are used to constrain the onset of the outburst. In Section 6, we apply several methods to determine the SMBH mass of SDSS J1105+1452 and its Eddington ratio. Section 7 explores the implications of the new MWL observations and provides a discussion of a variety of outburst scenarios. Section 8 provides a summary and conclusions, and sketches important future observations. Throughout this publication, we use a ΛCDM cosmological model with $H_0 = 70\ {\rm km\ s^{-1}\ Mpc^{-1}}$, $\Omega_{\rm m} = 0.3$, and $\Omega_\Lambda = 0.7$. At the redshift of SDSS J1105+1452, 1″ corresponds to a projected linear size of 2.18 kpc (E. L. Wright 2006).

2. Swift and ROSAT X-Ray Observations

2.1. Swift X-Ray Telescope

We have observed SDSS J1105+1452 eight times with the Neil Gehrels Swift Observatory (Swift hereafter; N. Gehrels et al. 2004) between October and December 2025 to measure its broadband X-ray spectrum for the first time and search for short-term variability among the Swift datasets and in comparison with the ROSAT detection in the 1990s. An archival Swift observation from 2023 October was added to the analysis. Exposure times range between 0.57 and 3.71 ks.

The Swift X-ray telescope (XRT; D. N. Burrows et al. 2005) was always operating in photon counting mode (J. E. Hill et al. 2004). The XRT data analysis was performed with the latest calibration files and using the `XRTDAS` package developed at the ASI Science Data Center, included in the `HEASoft` package (version 6.35.1). X-ray count rates were determined using the XRT product tool at the Swift data center in Leicester (P. A. Evans et al. 2007). Hardness ratios, $\mathrm{HR} = \frac{\mathrm{H-S}}{\mathrm{H+S}}$, were derived from the event file, and source and

[18] NLS1s are defined by FWHM(H$\beta_{\rm broad}$) < 2000 km s^{-1}, [O III]/Hβ < 3, and strong Fe II emission (D. E. Osterbrock & R. W. Pogge 1985; R. W. Goodrich 1989; M. P. Véron-Cetty et al. 2001).

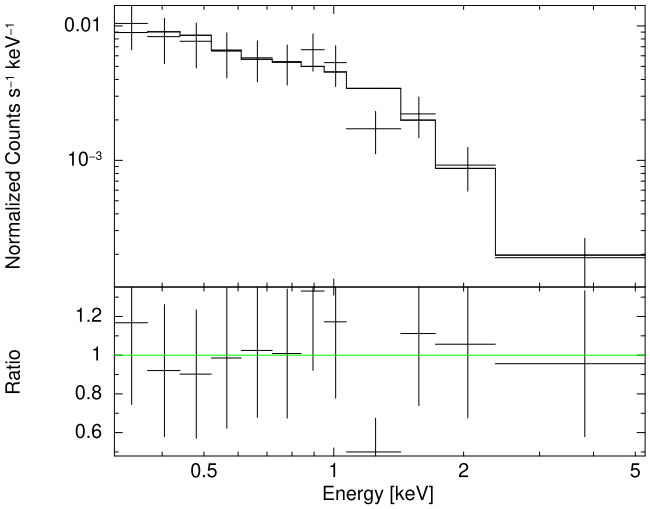

Figure 1. Merged Swift X-ray spectrum of SDSS J1105+1452, fit with a single power-law model (upper panel) and fit residuals (lower panel). The fit was performed on the unbinned spectrum; the spectrum shown here was binned for visualization purposes.

background counts were selected in the energy bands $S = (0.3–1.0)$ keV and $H = (1.0–10.0)$ keV. The hardness ratio was then determined by using the Bayesian estimation of hardness ratio method by T. Park et al. (2006). Source photons were extracted within a circular region with a radius of 20 detector pixels, where one pixel is equivalent to 2.″36. Background photons were collected in a nearby circular region of radius 236″. For spectral analysis, source and background spectra were created within `XSELECT`. Ancillary Response Files (ARFs) were generated, and the spectra were then binned with 1 ct bin^{-1}. We used the most recent response matrix `swxpc0to12s6-20210101v015.rmf`. All uncertainties are reported at the 1σ level.

The spectral analysis was then performed on the spectra in the (0.3–10) keV band using the software package `XSPEC` (version 12.15.0; K. A. Arnaud 1996). Since the source was too faint in single observations, the spectra from all the 2025 observations were merged. The ARFs were merged and weighted by their individual exposure time with respect to the total exposure time of the merged spectrum.

The combined and unbinned spectrum, with a total exposure time of 14.75 ks, was first fit with a single power-law model based on W statistics (W. Cash 1979). Galactic foreground absorption of a column density fixed at $N_{\rm H} = 1.32 \times 10^{20}$ cm^{-2} (HI4PI Collaboration et al. 2016) was included and modeled with `TBABS` (J. Wilms et al. 2000). This gives $\Gamma_{\rm X} = 2.51 \pm 0.16$ (Figure 1, Table 1). Next, the fit was repeated with $N_{\rm H}$ treated as an additional free parameter. In that case, the central value for the absorption slightly underpredicts the Galactic value, but within the uncertainties, it is unconstrained between 0 and 3.1×10^{20} cm^{-2}. Therefore, there is no evidence for excess absorption intrinsic to the galaxy. The fit with fixed Galactic absorption results in an absorbed (0.3–10) keV X-ray flux $f_{\rm abs} = (2.8 \pm 0.3) \times 10^{-13}$ erg cm^{-2} s^{-1}, an unabsorbed flux of $f = 3.0 \times 10^{-13}$ erg cm^{-2} s^{-1}, and a luminosity of 1.1×10^{43} erg s^{-1}.

2.2. Previous X-Ray Observations

SDSS J1105+1452 has previously been detected in the ROSAT all-sky survey (J. Truemper 1982) in 1990 with a ROSAT PSPC count rate of 0.087 cts s^{-1} in the energy band (0.1–2.4) keV (W. Voges et al. 1999; S. F. Anderson et al. 2007). Assuming the same spectral model as measured with Swift and Galactic absorption, this corresponds to an absorbed 0.3–10 keV flux of $f_{\rm abs,1990} = 6.0 \times 10^{-13}$ erg cm^{-2} s^{-1}. This implies long-term variability by a factor of 2 within 3.5 decades.

Table 1
X-ray Spectral Fit Results of the Combined 2025 XRT Data of SDSS J1105+1452

$N_{\rm H}$ 10^{20} cm^{-2}	$\Gamma_{\rm X}$	$f_{\rm int}$ [a] 10^{-13} erg s^{-1} cm^{-2}	$W_{\rm stat}$/d.o.f.
1.32 fixed	2.51±0.16	3.0 ± 0.3	0.86

[a] The absorption-corrected flux $f_{\rm int}$ is given in the band (0.3–10) keV.

3. Swift Ultraviolet/Optical Telescope Observations

We also observed SDSS J1105+1452 with the Swift Ultraviolet/Optical Telescope (UVOT; P. W. A. Roming et al. 2005) in all six optical and UV photometric bands with filters V (5468 Å), B (4392 Å), U (3465 Å), UVW1 (2600 Å), UVM2 (2246 Å), and UVW2 (1928 Å). Values in brackets represent the filters' central wavelengths (T. S. Poole et al. 2008).

UVOT observations were performed on the same dates as the XRT to measure the UV/optical spectral energy distribution (SED) and search for variability. Exposure times for the UVOT are in the same range as the XRT observations (Table 2). The UVOT filters V:B:U:W1:M2:W2 are nominally observed with a ratio of 1:1:1:2:3:4 of the total exposure time, respectively.

In each UVOT filter, the observations were first coadded using the tool `uvotimsum`. Source counts in all filters were then extracted in a circular region with a radius of 5″ centered on SDSS J1105+1452. The background was selected in a nearby region of 20″ radius. Using `uvotsource`, the background-corrected counts were then converted into VEGA magnitudes and into fluxes based on the latest calibration (T. S. Poole et al. 2008; A. A. Breeveld et al. 2010). The recently released `caldb` update, version 2024-02-01, was used. All fluxes are reported as flux density multiplied by the central frequency of the corresponding filter. A correction of the UVOT data for Galactic reddening was carried out assuming $E_{B-V} = 0.011$ mag (E. M. Schlegel 1990) and using a correction factor in each filter according to Equation (2) of P. W. A. Roming et al. (2005) and adopting the reddening curves of J. A. Cardelli et al. (1989). Within the uncertainties, the optical/UV emission of SDSS J1105+1452 is essentially constant (Figure 2).

4. Radio Observations

4.1. New Effelsberg Observations

In order to constrain the duration of the outburst and to measure the radio SED for the first time beyond a few GHz, new radio observations of SDSS J1105+1452 were obtained at the Effelsberg 100 m telescope based on a DDT proposal. Data acquired on 2025 August 4 were already reported in GKK25. Further observations were carried out between 2025 August and 2025 December (program-id 92-25), at frequencies

Table 2
Swift UVOT Observations of SDSS J1105+1452

Epoch	UVOT Exposure Time (s)	f_V	f_B	f_U	f_{W1}	f_{M2}	f_{W2}
2023-10-30	2404	19.3 ± 3.9	12.6 ± 2.3	11.2 ± 1.3	7.8 ± 0.7	10.2 ± 0.7	10.2 ± 0.7
2025-10-22	1601	24.1 ± 4.3	17.4 ± 2.6	8.9 ± 1.5	12.0 ± 1.2	13.7 ± 1.3	12.9 ± 0.9
2025-10-27	552	…	19.8 ± 2.9	10.6 ± 0.5	10.7 ± 1.0	…	…
2025-10-30	1341	22.2 ± 4.5	14.2 ± 2.4	11.7 ± 1.5	8.2 ± 1.1	12.1 ± 1.2	11.2 ± 0.9
2025-11-01	1649	25.2 ± 4.0	15.6 ± 2.1	12.0 ± 1.3	10.5 ± 1.0	11.2 ± 1.1	12.4 ± 0.8
2025-11-06	1733	20.6 ± 3.3	12.7 ± 2.0	11.3 ± 1.3	9.5 ± 0.9	12.5 ± 1.2	11.4 ± 0.9
2025-11-29	2319	22.0 ± 3.0	13.8 ± 1.5	12.01 ± 1.0	10.5 ± 0.9	11.1 ± 1.3	13.0 ± 0.7
2025-12-06	1774	25.9 ± 3.0	18.6 ± 1.8	11.8 ± 1.0	9.6 ± 0.8	10.2 ± 1.1	9.0 ± 0.8
2025-12-13	3710	22.2 ± 1.9	15.0 ± 1.1	11.6 ± 0.8	10.9 ± 0.7	11.1 ± 0.8	11.7 ± 0.7

Note. The UVOT fluxes, in 10^{-13} erg s^{-1} cm^{-2}, are corrected for Galactic extinction.

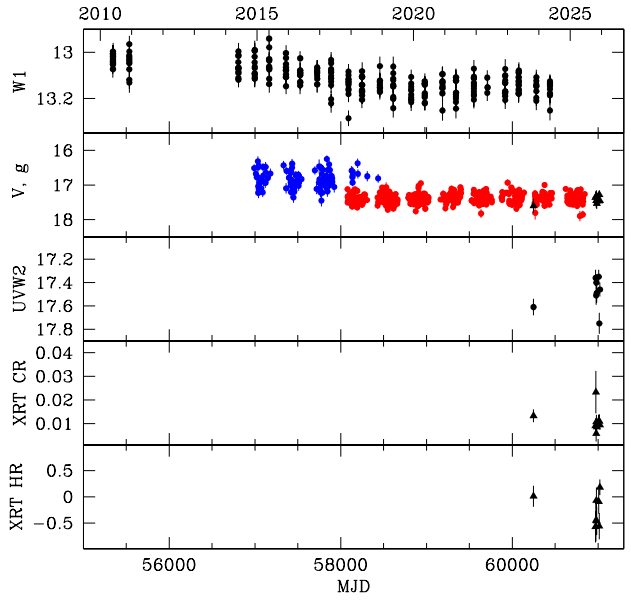

Figure 2. Long-term MWL light curve of SDSS J1105+1452 since 2010. Upper panel: WISE and NEOWISE W1 magnitudes. Second panel: ASAS-SN V (blue) and *g* (red) magnitudes (only detections are shown, no upper limits) and Swift V magnitude (black). Third panel: Swift UVW2 magnitude. Fourth panel: XRT count rate. Fifth panel: X-ray hardness ratio. The two POSS data points between 1949–1965 and 1985–2000, and the SDSS photometry of 2003 (Section 5.1) are not displayed.

between 4.85 and 16.75 GHz. A simultaneous SED of SDSS J1105+1452 between 4.85 and 16.75 GHz was measured for the first time in 2025 September. Higher-frequency observations were attempted, but were lost due to bad weather.

Observations were scheduled along with the target OJ 287 from one of our other observing programs (program-id 81-24; S. Komossa et al. 2023). These use the same receivers, and the two targets have similar sky locations. This approach allowed us to save observing time by sharing the calibrator sources and set-up.

Standard methods of data acquisition and data reduction (A. Kraus et al. 2003) were followed. The cross-scan method was used to obtain the radio data. In the cross-scans, the telescope was moved in two perpendicular directions, azimuth and elevation, with the position of SDSS J1105+1452 at the center of the scans. Due to the weakness of the source, at least 16 sub-scans (eight per scanning direction) were performed. All sub-scans of one direction were averaged to increase the signal-to-noise ratio, before, in a first analysis step, a Gaussian profile was fit to the data. In some instances, bad sub-scans (e.g., due to RFI) were identified and excluded from further analysis before the averaging process. After a correction for small pointing errors of the telescope, corrections for the opacity of the atmosphere were applied, as well as for the gain-elevation effect (the change of sensitivity with elevation). Finally, absolute flux calibration was achieved by comparing the observed antenna temperatures with the expected flux densities of calibrator sources like 3C 286. The measurement uncertainties are based on the errors resulting from the least squares fit of the Gaussian profiles and statistical errors from averaging of the data. These errors are propagated throughout the data reduction process and combined with a final contribution that reflects the apparent residual fluctuations of the calibrators.

The measurements (Table 3) show that the high state is still ongoing and has lasted at least 8 yr. The radio flux density at 4.85 GHz remains at $\geqslant$30 mJy. The radio spectrum of SDSS J1105+1452 declines steeply toward high frequencies. The radio emission is roughly constant. The monochromatic luminosity at 4.85 GHz is $L_{4.85\,\mathrm{GHz}} = 7 \times 10^{40}$ erg s^{-1}, and the ratio (Y. Terashima & A. S. Wilson 2003) $\log R_X = \log L_{4.85\,\mathrm{GHz}}/L_{(2-10)\mathrm{keV}} = -1.6$ (Table 4).

4.2. ATCA Observations

SDSS J1105+1452 was observed with the Australia Telescope Compact Array (ATCA) on 2025 December 21 between 21:30 and 22:30 UT and on January 7 between 14:00 and 15:00 UT (observation code CX601). ATCA, which consists of six 22 m diameter dishes, was in the east–west 6D array configuration at the time, with the shortest baseline of 77 m and the longest baseline of 5878 m. Observations were conducted in the 4 cm and 15 mm bands, where the new BIGCAT backend provides 4 × 1.92 GHz of bandwidth. The center frequencies of the four bands were 5.248, 7.168, 9.088, and 11.008 GHz in the 4 cm band, and 16.960, 18.880, 20.800, and 22.720 GHz in the 15 mm band. Ten minute observations of PKS B1934−638 were made in both bands for primary flux density calibration. Ten minute observations of SDSS J1105+1452 were bracketed by 2 minute scans on PKS 1055+018 for phase calibration.

BIGCAT data are recorded in LMA Science Data Model format. At the time of these observations, an observatory-developed bespoke version of CASA was used to convert the data to FITS format. Data reduction was then carried out in `Miriad` (R. J. Sault et al. 1995). Flux densities were

Table 3
Previous and New Radio Observations of SDSS J1105+1452.

Epoch	MJD	Survey/Telescope	Frequency (GHz)	Integrated Flux Density (mJy)	Beam Size (arcsec)	References
1986-05	⋯	GB6	4.85	$\lesssim$22	216 × 204	P. C. Gregory et al. (1996)
1994-06	⋯	NVSS	1.4	$\lesssim$2.5	45	J. J. Condon et al. (1998)
1999-12	⋯	FIRST	1.4	1.4 ± 0.1	5.4	D. J. Helfand et al. (2015)
2014-03-08	56724	GLEAM	0.2	< 45	⋯	N. Hurley-Walker et al. (2017)
2017-12-18	58105	VLASS	3	39.0 ± 0.4	2.5	GKK25
2020-04-30	58969	RACS-low	0.889	32.1 ± 2.8	25	C. L. Hale et al. (2021)
2020-08-18	59079	VLASS - SE	3	40.4 ± 0.4	2.5	GKK25
2021-01-04	59218	RACS-mid	1.367	32.4 ± 2.0	11.2 × 9.3	S. W. Duchesne et al. (2024)
2021-12-31	59579	RACS-high	1.655	42.7 ± 4.3	11.9 × 8.1	S. Duchesne et al. (2025)
2023-01-16	59960	VLASS	3	43.1 ± 0.5	2.5	GKK25
2025-08-04	60891	Effelsberg	4.95	32 ± 2	144	GKK25
	60891	Effelsberg	6.75	35 ± 2	84	GKK25
2018-06-12	58281	LoTSS	0.144	2.0 ± 0.2	6	This paper
2023-12-29	60307	RACS-low	0.944	36.1 ± 2.1	14.6 × 12.1	This paper
2024-01-25	60334	RACS-low	0.944	44.5 ± 2.5	14.7 × 12.8	This paper
2024-10-31	60614	RACS-mid	1.368	39.9 ± 2.3	12.8 × 8.8	This paper
2025-08-31	60918	Effelsberg	4.85	30 ± 5	145	This paper
2025-09-14	60932	Effelsberg	4.85	38 ± 2	145	This paper
	60932	Effelsberg	10.45	17 ± 2	67	This paper
	60932	Effelsberg	14.25	19 ± 3	53	This paper
	60932	Effelsberg	16.75	18 ± 2	44	This paper
2025-10-25	60973	FLASH	0.856	28.8 ± 1. 7*	23.1 × 13.2	*Uncertain; see Section 4.3.3
2025-11-04	60983	Effelsberg	14.25	15 ± 3	53	This paper
	60983	Effelsberg	16.75	12 ± 3	44	This paper
2025-12-21	61030	ATCA	5.248	26 ± 4	458 × 1.4	This paper
	61030	ATCA	7.168	23 ± 4	339 × 1.0	This paper
	61030	ATCA	9.088	13 ± 4	268 × 0.8	This paper
	61030	ATCA	11.008	8 ± 3	224 × 0.6	This paper
	61030	ATCA	16.960	4 ± 2	112 × 0.5	This paper
	61030	ATCA	18.880	<4	102 × 0.4	This paper
	61030	ATCA	20.800	<4	94 × 0.4	This paper
	61030	ATCA	22.720	<4	85 × 0.4	This paper
2025-12-22	61031	Effelsberg	4.83	32 ± 2	145	This paper
	61031	Effelsberg	6.67	30 ± 3	84	This paper
	61031	Effelsberg	10.45	18 ± 2	67	This paper
2026-01-07	61047	ATCA	5.248	31 ± 4	195 × 2.1	This paper
	61047	ATCA	7.168	24 ± 3	143 × 1.6	This paper
	61047	ATCA	9.088	19 ± 2	114 × 1.2	This paper
	61047	ATCA	11.008	15 ± 2	93 × 1.0	This paper
	61047	ATCA	16.960	2 ± 1	63 × 0.6	This paper
	61047	ATCA	18.880	<3	57 × 0.5	This paper
	61047	ATCA	20.800	<4	52 × 0.5	This paper
	61047	ATCA	22.720	<4	47 × 0.4	This paper

Table 4
Summary of the Radio Properties of SDSS J1105+1452

$t_{\rm rise,radio}$ yr	$t_{\rm high\text{-}state}$ yr	$A_{1.4\ \rm GHz}$	$L_{4.85\ \rm GHz}$ erg s^{-1}	$\log R_{\rm X}$
<18	>8.1	>23	$7\ 10^{40}$	−1.6

Note. Column (1) Observed rise timescale $t_{\rm rise,radio}$ in the radio band based on the FIRST radio low-state and the first VLASS high-state detection. Column (2) Duration $t_{\rm high\text{-}state}$ of the high state. Column (3) Amplitude $A_{1.4\ \rm GHz}$ of variability at 1.4 GHz. Column (4) monochromatic 4.85 GHz high-state luminosity $L_{4.85\ \rm GHz}$. Column (5) Log of the ratio $R_{\rm X}$ of $L_{4.85\ \rm GHz}$ over $L_{(2-10)\ \rm keV}$.

measured in both the $uv-$ and image plane, using a combination of the `uvfmeas` routine, and imaging with `robust = 0.5`.

SDSS J1105+1452 is still in its high state during the latest measurements of 2026 January (Table 3). It is not detected at frequencies >18 GHz that are measured with ATCA for the first time, with upper limits of <4 mJy. The spectral index α, defined as in $f_\nu \propto \nu^\alpha$, is $\alpha_{\rm thin} = -1.3 \pm 0.3$ in the 4 cm band for the observations between December and January.

4.3. Archival radio Observations

4.3.1. LOFAR Observations

SDSS J1105+1452 was observed seven times at 144 MHz between 2018 and 2024 as part of observations for the third data release (DR3) of the Low Frequency Array (LOFAR) wide-area survey of the northern sky, LoTSS (T. W. Shimwell et al. 2026). The source is clearly detected at a flux density of ∼2 mJy in the LoTSS DR3 mosaics.

Because of the survey tiling strategy of LoTSS, many of the individual 8 hr observations that cover the source see it only at a large distance from the pointing center and therefore do not allow a good-quality flux density measurement. However, the source is only 0.45° from the pointing center of field P166+15, which was observed for 8 hr on 2018 June 12, and this allows a measurement of 2 ± 0.2 mJy at this epoch. The other available observations do not provide any statistically significant detections, but are consistent with this flux density and allow us to rule out a strong increase in flux by the end of the observing period (e.g., the flux density is < 3 mJy at 5σ confidence in the observation of field P163+17 on 2024 February 26).

4.3.2. ASKAP Observations

We searched the CSIRO ASKAP Science Data Archive (CASDA; M. Huynh et al. 2020) for significant ($\geqslant 5 \times$ rms) detections in ASKAP catalogs within 5″ of SDSS J1105+1452's position. We identified several detections from the Rapid ASKAP Continuum Survey (RACS; C. L. Hale et al. 2021; S. W. Duchesne et al. 2024; S. Duchesne et al. 2025) at frequencies between 0.944 and 1.368 GHz and the First Large Absorption Survey in H I (FLASH; H. Yoon et al. 2025) at 0.856 GHz. Flux density measurements were extracted using the `Selavy` source-finding method implemented in the ASKAP processing pipeline; see M. Whiting & B. Humphreys (2012) for details. For conservative flux uncertainties, we took a quadrature sum of the image rms, the fitted `Selavy` peak flux error, and a 6% flux scaling error. Results show that the source was in the high state during all these observations taken between 2023 and 2025 (Table 3).

4.3.3. Further Archival Data

Table 3 also lists additional radio observations from GKK25. These are based on the catalogs of the Green Bank 6 cm survey (GB6; P. C. Gregory et al. 1996), the NRAO VLA Sky Survey (NVSS; J. J. Condon et al. 1998), the FIRST survey (R. L. White et al. 1997), the Very Large Array Sky Survey (VLASS; M. Lacy et al. 2020), and the RACS (D. McConnell et al. 2020). In addition, we have obtained an upper limit on the 200 MHz flux density from the GaLactic and Extragalactic All-sky Murchison Widefield Array (GLEAM) survey image archive (N. Hurley-Walker et al. 2017) of < 45 mJy. SDSS J1105+1452 was not detected in the 1980s and 1990s in GB6 and NVSS, and was faint in FIRST (1.4 mJy)[19]. It has been in the radio high state since the VLASS observation in 2017.96 (Figure 3).

Overall, the high-state radio emission is roughly constant at a ∼10% uncertainty level, with the exception of the FLASH measurement (field SB 78421), flagged uncertain in the archive database. According to the validation report,[20] flux densities in the whole field are systematically low by ∼13%. The power-law spectral index $\alpha_{\rm thick}$ was determined for the low-frequency part of the radio SED based on the three RACS-low measurements and LoTSS between 0.9 and 0.14 GHz. This gives $\alpha_{\rm thick} = 1.6 \pm 0.1$.

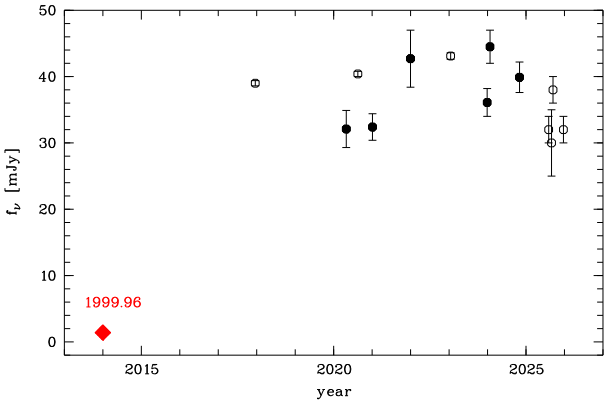

Figure 3. Radio light curve of SDSS J1105+1452. The leftmost red diamond represents the FIRST low-state data point of 1999.96 (not to scale on the time axis but added for visualization purposes). The more recent high-state data points at all frequencies between 0.8 and 1.7 GHz are shown as filled black circles, and the high-state data points at frequencies between 3 and 5 GHz are represented with open circles. The high-state radio emission since December 2017 has been roughly constant at fixed frequency and already lasted for >8 yr.

5. Archival Optical and IR Observations

5.1. Long-term Optical and IR Photometry

To constrain the onset of the radio outburst that must have happened between 1999.96 (FIRST low state) and 2017.96 (VLASS high state), we have inspected archival optical and IR photometric databases in search of high-amplitude variability (from either the accretion disk, which could have triggered the change in jet emission, or directly from the increase in nonthermal jet emission itself if extending into the IR/optical regime). Data prior to 2017.96 are of special interest in constraining the rise phase. Several photometric surveys cover these epochs.

All-Sky Automated Survey for Supernovae. SDSS J1105+1452 has been frequently observed in the course of the All-Sky Automated Survey for Supernovae (ASAS-SN; B. J. Shappee et al. 2014; C. S. Kochanek et al. 2017) since 2014[21] at a cadence of several days and with gaps of 3–4 months each year when the object is too close to the Sun. In Figure 2, we show the Johnson *V*-band and Sloan *g*-band light curve using coadded data (3 frames per epoch) and image subtraction, including all data points with photometric uncertainties $\leqslant \pm 0.10$ mag. Magnitudes are the integrated magnitudes within an aperture of 16″ and include the host galaxy contribution.

The median *g*-band magnitude is 17.4, and the median *V*-band magnitude is 17.09. SDSS J1105+1452 does not show any systematic changes that could correspond to the factor of ∼20 increase in the radio regime.

Zwicky Transient Factory. SDSSJ1105+1452 has also been observed with the Zwicky Transient Factory (ZTF) since 2018 in the three filter bands *r*, *g*, and *i* (E. C. Bellm et al. 2019; F. J. Masci et al. 2019). We have retrieved the publicly available point spread function (PSF) magnitudes (between

[19] The GB6, NVSS, and FIRST survey observations extended over a period of months to years, and the mid-epochs were assigned as observation dates in the literature (Table 3); 1999.96 in the case of FIRST (D. J. Helfand et al. 2015).

[20] https://ingest.pawsey.org.au/casda-support-files/validation/ASKAP/78421/AS209/validation_image.i.FLASH_667.SB 78421.cont.taylor.0.restored.conv/index.html

[21] https://asas-sn.osu.edu/

MJD 55203 and 57054),[22] then filtered out data taken under unfavorable conditions, and inspected the remaining ones for any high-amplitude variability that could represent an outburst in the ZTF bands. None is found, consistent with the conclusions drawn from the ASAS-SN light curve.

Catalina Sky Survey. The Catalina survey (A. J. Drake et al. 2009) has occasionally covered the position of SDSS J1105 +1452 since the year 2007. The light curve was inspected, and no systematic change in the optical magnitude was found.

SDSS Photometry. SDSS J1105+1452 was observed twice with SDSS (D. G. York et al. 2000). The spectrum was taken on 2005 January 7. The photometry was carried out earlier on 2003 January 28. This represents an early optical photometric dataset to be inspected for a change in the optical band that could signal the onset of the radio outburst. The integrated SDSS g magnitude of 17.7 $\pm$ 0.01 (J. K. Adelman-McCarthy et al. 2009) agrees well with the average ASAS-SN g magnitude of 17.4 $\pm$ 0.2. The same agreement is found when comparing the PSF magnitudes of the core. The SDSS PSF g-band magnitude of 18.6 (S. F. Anderson et al. 2007) is consistent with the average ZTF g-band magnitude of 18.3 $\pm$ 0.1. This result shows that a major change in optical emission is absent.

POSS-I and II. Photometry of SDSS J1105+1452 (D. G. Monet et al. 2003) was also performed in the course of POSS-I (Palomar Observatory Sky Survey; 1949–1965) and POSS-II (1985–2000). While these observations precede the FIRST low-state data point by up to ~50 yr, they still give an impression of the past variability of SDSS J1105+1452,[23] which is very high in the blue band. During POSS-I, $m_{\rm O,I} = 18.10$, and during POSS-II, $m_{\rm J,II} = 15.78$, with an uncertainty of ~0.25 mag, or $m_{\rm O,II} = 16.02$ after a correction owing to the different plate emulsions, O and J, used during the two surveys, respectively (D. G. Monet et al. 2003). This large magnitude difference corresponds to a factor $\geqslant$6.8 flux variability, and given only two available epochs, the total amplitude may have well been much higher.

Given these available constraints, we cannot tell whether this high-amplitude variability was the trigger event for the (delayed) radio turn-on, or was an earlier, unrelated event. In any case, it does show that SDSS J1105+1452 is capable of undergoing high-amplitude optical continuum variability.

WISE and NEOWISE. In the IR, SDSS J1105+1452 was observed with the Wide-field Infrared Survey Explorer (WISE, E. L. Wright et al. 2010) in the bands W1–W4 centered on 3.4, 4.6, 12, and 22μm, respectively. Observations taken during WISE and the more recent NEOWISE survey (A. Mainzer et al. 2014) between 2010 and 2024 were retrieved from the NASA/IPAC Infrared Science Archive.[24] Measurements with lower photometric quality were excluded (GKK25). The only variability seen in the IR bands is a mild decrease in flux density, shown in Figure 2.

5.2. Optical image

The SDSS image[25] of SDSS J1105+1452 shows a spiral galaxy and an additional point source at ~6″ from the galaxy center. The DESI legacy survey image[26] (A. Dey et al. 2019) goes deeper and reveals the outer spiral arms and additional sources in the field (Figure 4). The low-state and high-state radio emission (D. J. Helfand et al. 2015; Y. A. Gordon et al. 2021) arises from the center of the galaxy and is not associated with the off-nuclear point sources (Figure 4; where the VLASS radio position is the most accurate high-state position). The FIRST low-state and VLASS high-state positional uncertainties are 1″ and 0″.5, respectively. VLASS agrees with the optical position of SDSS J1105+1452 within 0″.3 (Gaia DR3; Gaia Collaboration et al. 2023; P. Gavras et al. 2023).

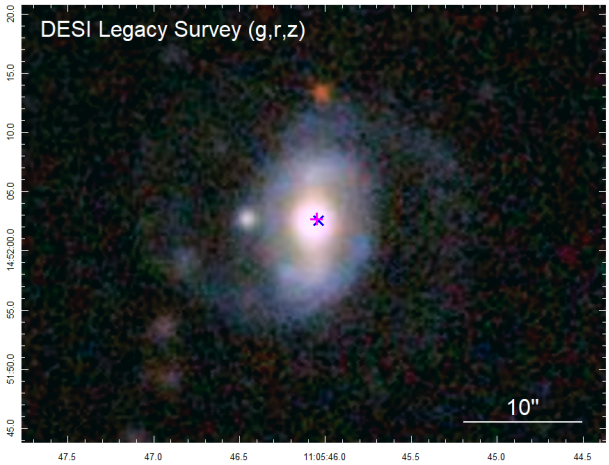

Figure 4. Multicolor DESI image of the barred spiral galaxy SDSS J1105 +1452. The radio emission coincides with the center of the galaxy (blue cross: FIRST low-state, magenta plus: VLASS high state).

6. SMBH Mass Estimates, Eddington Ratio, and NLS1 Classification

6.1. SMBH Mass and Eddington Ratio

In the course of several SDSS large-sample studies, the SMBH mass of SDSS J1105+1452 was estimated employing the 5100 Å continuum luminosity, the FWHM of Hβ, and broad-line region (BLR)–SMBH single-epoch scaling relations. This approach consistently resulted in $M_{\rm BH} < 10^7\ M_\odot$ (J. Sun & Y. Shen 2015; S. Rakshit et al. 2017; V. S. Paliya et al. 2024). Given that the optical continuum emission may have a significant contribution from nonthermal jet emission, we alternatively use the Hβ luminosity to derive the SMBH mass (M. Vestergaard & B. M. Peterson 2006). With $L({\rm H}\beta) = 10^{41.40}$ erg s^{-1} (G. Viswanath et al. 2019; see also K. Oh et al. 2015) and

$$M_{\rm BH} = 10^{6.67} \left(\frac{L_{\rm H\beta}}{10^{42}\ {\rm erg\ s^{-1}}}\right)^{0.63} \left(\frac{\rm FWHM(H\beta)}{1000\ {\rm km\ s^{-1}}}\right)^2 M_\odot, \quad (1)$$

one obtains $M_{\rm BH} = 4.4 \times 10^6\ M_\odot$. With $L_{\rm Edd} = 1.3 \times 10^{38} M_{\rm BH}/M_\odot$ erg s^{-1} and $L_{\rm bol} \simeq 10 \times L_{\rm X} = 1.1 \times 10^{44}$ erg s^{-1} (M. Elvis et al. 1994; D. Grupe et al. 2010), this then gives an Eddington ratio *of* $\lambda_{\rm Edd} = L_{\rm bol}/L_{\rm Edd} = 0.2$.

M. Vestergaard & B. M. Peterson (2006) estimate an uncertainty of 0.5 dex for single-epoch SMBH mass values. Within this uncertainty, the SMBH mass alternatively derived from Hα width and luminosity (S. Rakshit et al. 2017)

[22] https://irsa.ipac.caltech.edu/cgi-bin/Gator/nph-scan?mission=irsa&submit=Select&projshort=ZTF accessed 2026 January 14.
[23] Note that the exact observation dates of any object during POSS-I and II are not known (D. G. Monet et al. 2003).
[24] irsa.ipac.caltech.edu accessed 2025 August 2.
[25] skyserver.sdss.org/dr14/en/tools/explore/summary.aspx? accessed 2025 Oct 1.
[26] skyserver.sdss.org/dr14/en/tools/explore/summary.aspx?

measurements and applying one of the single-epoch relations for Hα (E. Dalla Bontà et al. 2025) is consistent with the Hβ-based value. We prefer the Hβ relation because of the extra uncertainty in deblending Hα from [N II].

Alternatively, the SMBH mass can be measured from the host galaxy stellar velocity dispersion σ_*. Using $\sigma_* = 82$ km s^{-1} (J. Sun & Y. Shen 2015) and the $M_{\rm BH}$–σ_* relation of nonelliptical galaxies (K. Gültekin et al. 2009),

$$\log M_{\rm BH} = 8.01 + 4.05 \log\left(\frac{\sigma_*}{200 \text{ km s}^{-1}}\right), \quad (2)$$

then gives $M_{\rm BH} = 2.8 \times 10^6\ M_\odot$ and $\lambda_{\rm Edd} = 0.3$.

6.2. NLS1 Classification

The optical spectrum of SDSS J1105+1452 fulfills all three classification criteria of an NLS1 galaxy (Section 1). Alternatively, in the main-sequence classification scheme of P. Marziani et al. (2018), SDSS J1105+1452 is in the regime of (extreme) population A sources based on its strong Fe II emission and FWHM(Hβ). This regime corresponds to NLS1 galaxies.

Further properties of SDSS J1105+1452, the SMBH mass, Eddington ratio, and the soft X-ray spectrum, are consistent with its optical NLS1 classification, demonstrating that its NLS1 nature is very well established. This is important because variable radio emission, radio-loudness, and optical changing-look events are all relatively rare in NLS1 galaxies, and therefore the NLS1 classification of SDSS J1105+1452 and its SMBH mass have to be carefully evaluated.

7. Discussion

SDSS J1105+1452 is rare in its high amplitude of radio variability and unique in its outburst duration. Here, we first discuss constraints from the new MWL observations and then turn to outburst scenarios.

7.1. X-Ray Spectrum

The X-ray spectrum is relatively steep with a photon index of $\Gamma_{\rm X} = 2.5$, suggesting the presence of a soft X-ray spectral component frequently observed in NLS1 galaxies (E. M. Puchnarewicz et al. 1992; D. Grupe et al. 2010). Indeed, the residuals we see in the X-ray spectral fit could indicate the intersection of two components; however, SDSS J1105+1452 is too faint in X-rays for Swift to allow the fit of two-component models. The fact that the X-ray emission was brighter in the soft (0.1–2.4) keV ROSAT band is consistent with variable accretion disk-related emission as well. The soft X-ray spectrum is well consistent with the NLS1 nature of SDSS J1105+1452.

7.2. Extinction and Absorption

X-ray and optical observations can be used to measure the absorption and extinction along our line of sight (LOS). This information is important for the evaluation of turn-on scenarios, and also for the radio-loudness measurement of SDSS J1105+1452. The radio-loudness index (K. I. Kellermann et al. 1989) is only well defined for unabsorbed AGN.

The galaxy has a blue continuum and is detected in the UV, implying a lack of heavy extinction. The Balmer decrement of the BLR, the flux ratio $f(\text{H}\alpha)/f(\text{H}\beta) = 3.3$, is close to the case B recombination value (D. E. Osterbrock 1989) and implies that there is little dust extinction along our LOS. Assuming an intrinsic value of $f(\text{H}\alpha)/f(\text{H}\beta) = 3.1$ (often used to represent the intrinsic emission) and a Galactic reddening law, we obtain a reddening of $E(B-V) = 0.05$. Using the case B value for the Balmer decrement of 2.85 (D. E. Osterbrock 1989; C. M. Gaskell 2017) gives $E(B-V) = 0.12$.

A Galactic gas/dust composition then implies a column density of cold hydrogen of $N_{\rm H} = 1.79 \times 10^{21} \times A_{\rm V}$ (P. Predehl & J. H. M. M. Schmitt 1995), where $A_V = 3.1 \times E(B-V)$, and in the case of SDSS J1105+1452 $N_{\rm H} = 2.8 \times 10^{20}$ cm^{-2}. This value is an upper limit since the Balmer decrement can also be affected by optical depth effects intrinsic to the BLR.

The X-ray spectral fits do not require excess absorption either, and only allow for at most a small amount of intrinsic absorption, $<3.1 \times 10^{20}$ cm^{-2}.

7.3. Constraints on a Starburst Contribution

The starburst contribution in the IR/optical regime can be estimated in several different ways. It is important for assessing the broadband properties and evolutionary state of SDSS J1105+1452 in general, and its variability characteristics in particular. First, the WISE IR colors locate SDSS J1105+1452 in the AGN regime of the IR color–color diagram (GKK25; T. H. Jarrett et al. 2011, their Figure 26). Second, the faintness of [O II]3727 versus [O III]5007 in the SDSS spectrum implies that narrow emission-line ratios are not dominated by star formation. Third, converting the star formation rate measured from the MWL SED, of only 2 $M_\odot$ yr^{-1} (R. S. Barrows et al. 2021), into the associated 1.4 GHz radio emission (A. M. Hopkins et al. 2003), we predict a luminosity $L_{1.4\,\rm GHz,\ SF} = 3.6 \times 10^{21}$ W Hz^{-1}. This value is 15 times *lower* than the actually observed FIRST low-state radio emission. It implies that the emission arises from AGN activity rather than star formation.

7.4. SED

The broadband SED shown in Figure 5 is based on the simultaneous Effelsberg measurements, the RACS observation from 2024, the latest NEOWISE measurements, the Swift UVOT observation in 2025 November, and the merged Swift XRT spectrum. The 0.8–20 GHz radio spectrum (Figure 6) is broadly similar to gigahertz-peaked-spectrum (GPS) radio sources (C. P. O'Dea 1998). These are interpreted as young radio jets less than approximately thousands of years old. Two main mechanisms are thought to be responsible for the spectral turnover in GPS sources (see reviews by C. P. O'Dea 1998; C. P. O'Dea & D. J. Saikia 2021), synchrotron self-absorption (SSA) and free-free absorption (FFA). In SSA, the turnover frequency depends on internal properties (e.g., the magnetic field and electron density). An anticorrelation between source size and turnover frequency is observed (C. P. O'Dea & S. A. Baum 1997). In FFA, the turnover frequency depends on properties of the external medium (e.g., the density of thermal electrons) the jet is interacting with (G. V. Bicknell et al. 2018), such as a BLR or narrow-line region (NLR) cloud. The spectra of GPS sources decline steeply toward both lower frequencies (the optically thick part of the SED) and higher frequencies (the optically thin part). The majority of GPS sources show little radio variability (C. P. O'Dea & D. J. Saikia 2021) and are hosted by large elliptical galaxies

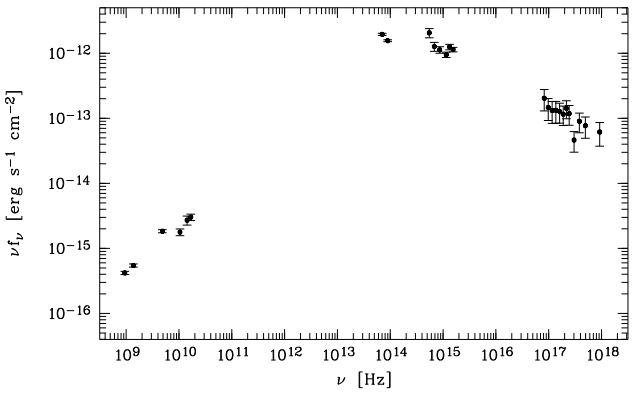

Figure 5. Broadband SED of SDSS J1105+1452 from radio to X-rays based on data from RACS, Effelsberg, NEOWISE, Swift UVOT, and Swift XRT.

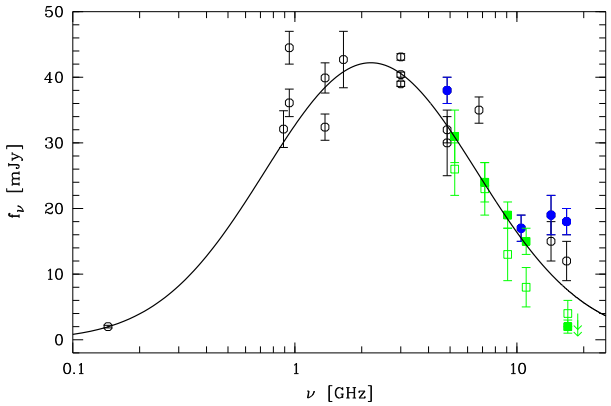

Figure 6. High-state radio SED of SDSS J1105+1452. Simultaneous radio observations taken in September 2025 with the Effelsberg 100 m telescope are marked with filled blue circles, simultaneous ATCA measurements are shown with open green squares (2025 December) and filled green squares (2026 January). Other flux density measurements are shown with open circles. The best-fit log-space parabola is shown with a black line.

with old stellar populations (W. H. de Vries et al. 2000), but a fraction of NLS1 galaxies is known to host compact radio sources with peaked spectra as well.

The turnover frequency of SDSS J1105+1452 is clearly located at low frequencies. To determine the turnover value, a parabola of the form $\log y = c\ (\log x)^2 + b \log x + a$ was fit to the SED employing `RadioSED`[27] (E. F. Kerrison et al. 2024), where x is the frequency in MHz and y is the flux density in Jy. The SED is well fit by this function, with coefficients $a = -11.94^{+0.23}_{-0.25}$, $b = 6.35^{+0.15}_{-0.14}$, and $c = -0.95^{+0.02}_{-0.02}$ (Figure 6). This then implies a turnover frequency of 2.1 GHz.

At a turnover frequency of 2 GHz, the turnover-size relation (C. P. O'Dea 1998) would imply a jet size of ∼0.1–0.2 kpc of SDSS J1105+1452. On the other hand, a very young jet, only several years old (as observed), or ∼10 pc in size and launched for the first time, would show a much higher turnover frequency >10 GHz within this specific scenario (C. P. O'Dea 1998; K. Nyland et al. 2020). However, multiple parameters could affect the SED shape of SDSS J1105+1452. It could be peaked at low(er) frequency because an event (like a change in accretion rate) triggered a wider-angle jet or outflow, or because the magnetic field of SDSS J1105+1452 was lower than GPS sources as a class, thus shifting the synchrotron peak to lower frequencies. The spatial resolution of VLASS, 2.″5 limits the linear size of the jet of SDSS J1105+1452 to <5.4 kpc.

We come back to variants of SSA and FFA scenarios in Section 7.6. We also note that in the case of exceptional new transients like SDSS J1105+1452, the observed low-frequency decline does not need to be associated with any absorption processes, but could alternatively represent the intrinsic energy distribution of the ejected electron population, with a lack of low-energy electrons.

Significant radio variability is absent. Small deviations at a roughly $\lesssim$10%−20% level could be due to interstellar scintillation (P. J. Hancock et al. 2019), a small extent of the radio emission (the bulk is pointlike) in combination with the different spatial resolutions of the surveys and instruments, and/or a small underestimate of the measurement uncertainties.

7.5. Timing of the Turn-on

Radio observations place the epoch of the rise phase between 1999.96 (the FIRST low-state) and 2017.96 (the VLASS high state). It is plausible to assume that the turn-on also affected the IR/optical band either by accretion disk variability that triggered the jet change, and/or by the synchrotron emission itself extending into the IR/optical band. Therefore, we have inspected available MWL surveys in search of a factor of ∼20 (or any systematic[28]) change in the flux level. We did not detect any. In the IR, WISE dates back to 2010. In the optical, ASAS-SN dates back to 2014, the Catalina survey back to 2007, and SDSS photometry back to 2003. Therefore, if the radio turn-on was accompanied by a significant optical/IR change, the trigger likely occurred before 2003.

Is there any possibility that the turn-on could have happened later (i.e., between 2003 and 2017.96), but we did not detect it in the IR and optical bands? First, one might speculate that absorption and extinction affected the X-ray, IR, and optical bands, making any turn-on undetectable in those bands. This scenario can be tested by measuring the LOS extinction from the BLR Balmer decrement and the X-ray absorption from the spectral fit. No significant absorption is detected either way (Section 7.2), and we therefore reject this scenario. Next, we raise the question of whether a change in emission could have been hidden in the IR/optical by a strong star formation component, such that its change was present but remained undetected. However, as discussed above (Section 7.3), the IR emission is dominated by the AGN.

Finally, we note that owing to the lack of dense X-ray coverage, one cannot yet exclude the possibility that an earlier, pre-1999.96, change of the inner accretion disk, e.g., as traced by the higher X-ray state observed during the RASS in 1990 and/or by the higher blue magnitude during POSS, already triggered the jet launch but a significant rise in radio emission only occurred years later (between 1999.96 and 2017.96) after the jet encountered and shocked high-density material.

[27] https://github.com/ekerrison/RadioSED

[28] Note that in the absence of detailed disk-jet modeling, it is a priori unknown whether an *increase* or *decrease* in accretion rate would trigger an increase in radio jet emission, or whether any other reconfiguration in the disk structure and/or emission not directly linked to the accretion rate affected magnetic flux accumulation. Further, it is possible that there is a time delay between the accretion disk change observed in optical-X-ray emission and the detection of radio jet emission.

7.6. Outburst Scenarios

The coincidence of the radio source with the center of the galaxy strongly suggests a link between the radio outburst and nuclear activity. However, among NLS1s and other types of AGN, the radio properties of SDSS J1105+1452 are unique, and none has shown such a high-amplitude and long-lasting radio outburst at low frequencies before. The different scenarios can be sorted into different categories: (1) Outbursting compact sources unrelated to the SMBH environment, like radio supernovae, are not discussed here further since the radio-brightest ones known are still factors ∼100 less luminous than SDSS J1105+1452 (e.g., F. Zhang et al. 2022). (2) Extrinsic variability caused by gravitational lensing or by absorption, or magnification due to beaming. (3) Intrinsic variability triggered in the SMBH environment. There are three main processes thought to affect jet launching: First, accretion disk variability, including catastrophic events like TDEs. Second, (a change in) black hole spin. A spin change is difficult to achieve on short timescales, except for a merger with a second SMBH. Third, changes in magnetic flux accumulation near the horizon. Below, we discuss these different scenarios using constraints from the many MWL observations of SDSS J1105+1452.

7.6.1. Gravitational Lensing

Lensing of a compact radio knot can enhance the radio emission if a lens at a suitable location along the LOS exists. We have carefully inspected the host galaxy image and optical spectrum of SDSS J1105+1452. Neither do we recognize evidence for any foreground galaxy in the image, nor is there a second emission-line system with a different redshift in the optical spectrum that could indicate the presence of a lens.

7.6.2. Absorption Variability

H I absorption variability. This scenario considers absorption variability and assumes that the high state rather represents the "normal" state, and the low state was due to an extreme absorption event. In this scenario, the early FIRST and NVSS observations at 1.4 GHz would have been severely affected by H I 21 cm absorption. For this mechanism to work, one has to assume a compact jet shielded by a BLR cloud or torus clump along our LOS. The radio flux is diminished as S (1.4, low) = S(1.4, high) $e^{-\tau}$, where τ is the optical depth. τ depends on the gas column density and spin temperature T_s. At typical BLR column densities $>10^{23-24}$ cm^{-2} (H. Netzer 2013; S. Panda 2021), the optical depth can be significant. However, at the redshift of SDSS J1105+1452, 21 cm absorption would be centered at 1.25 GHz and could extend into the FIRST and NVSS band only at a high BLR velocity dispersion of a few 10,000 km s^{-1}, not expected for the wings of the BLR profile of an NLS1 galaxy. Further, the 4.85 GHz band should not be affected, but the GB6 data still show a significantly lower radio flux than the recent Effelsberg and ATCA observations at the same frequency. Further, there is no other evidence for strong absorption along our LOS. For instance, the RASS detection in the soft X-ray band (several years before the NVSS nondetection) implies the absence of such high gas column densities along our LOS at that epoch.

FFA by an extended or compact ionized medium. In this scenario, a steady jet that has formed in the past centuries or millennia traversing ionized material (absent along our LOS to the accretion disk region; see MWL absorption constraints in Section 7.2) is subject to FFA. The free-free optical depth is given by $\tau_{\rm ff} \simeq 0.082\,(T/{\rm K})^{-1.35}\,(\nu/{\rm GHz})^{-2.1}\,{\rm EM}/({\rm pc\,cm^{-6}})$ (P. G. Mezger & A. P. Henderson 1967). A decrease in emission measure (EM) could then explain the rise at low frequencies. However, this scenario would require a relatively sharp edge of the absorber, and across a significant part of the width of a jet or lobe, to explain the rapid rise within only decades. It also predicts strong changes in spectra and fluxes as the absorbing medium clears, in addition to light travel time delays across a jet with an opening angle of a few light years to a few dozen light years, which are not observed. If, instead, only a small fraction of the whole jet broke free, the high amplitude of variability and high radio luminosity in the radio-loud regime would be surprising, and it would imply an even higher total amplitude of variability. Sharp gas-cloud boundaries are more naturally encountered in the dense core environment, when a newly launched, more confined jet passes through an ionized high-density cloud. For instance, at $v \simeq c$, a new jet component could reach a coronal-line region (CLR) cloud after 1 yr. At a typical CLR cloud column density of $N_{\rm H} = 10^{22}$ cm^{-2} and a density of 10^6 cm^{-3} (J. W. Ferguson et al. 1997), the whole cloud of dimension 10^{16} cm can be crossed in days, well consistent with the rise time of <18 yr. The high-state duration of >8 yr then implies that no other dense material was encountered. This is possible for a low covering fraction of the CLR. However, at a typical jet opening angle of ∼1 lt-yr and a cloud dimension of $\sim 10^{-2}$ lt-yr, only a small fraction of the jet would be subject to FFA, implying a giant total amplitude of variability to raise the integrated luminosity by a factor of 23. Further, the question regarding the initial trigger mechanism of such a newly launched jet component remains unanswered in this scenario.

SSA in the core region. One can speculate that jet activity is intermittent (C. S. Reynolds & M. C. Begelman 1997; M. Kunert-Bajraszewska et al. 2011) and a new jet component of SDSS J1105+1452 was recently launched (due to an unspecified trigger mechanism). If initially dense and compact, the blob would experience SSA such that the few GHz region was highly optically thick in the 1980s and 1990s but became optically thin afterward, leading to a shift of the Synchrotron peak to lower frequencies and therefore to a rapid rise in the observed low-frequency radio emission. The question is then raised, why the radio spectrum would evolve very rapidly, from ∼10 GHz-peaked to 2 GHz-peaked within years, whereas this evolution usually takes centuries to millennia in known GPS sources (C. P. O'Dea 1998). Rapid expansion in the absence of a dense confining medium could be a possibility (see also Section 7.4). However, first, if the overall high-frequency (∼10 GHz) radio emission only increased mildly due to the new blob, then we would still expect the emission from older optically thin components to extend into the 1–2 GHz band, effectively leading to only mild variability at low frequency (which is not the case). If instead, the 10 GHz flux increased by a high factor, we would still require high-amplitude variability in radio flux in the first place, and the question about the trigger mechanism remains.

7.6.3. Binary SMBH Jet Swing, or Spin Flip Following Coalescence

A jet crossing the observer's LOS due to precession caused by the presence of a binary SMBH (or by other jet processes) could lead to a radio outburst due to temporary Doppler

boosting. Alternatively, binary SMBH coalescence could lead to a newly formed inner accretion disk around the single SMBH different from the precoalescence circumbinary disk (D. J. D'Orazio et al. 2013) on a timescale of $\sim 7\ (1+z)\ (M/10^6\ M_\odot)$ yr (M. Milosavljević & E. S. Phinney 2005) with different jet properties, or it could lead to a spin flip of the newly formed single SMBH (M. Campanelli et al. 2007) and therefore launch a new jet in a new direction. This latter scenario is attractive because high-amplitude variability, a drop and re-rise, is only expected for the inner (X-ray emitting) disk, the evolution is rapid for low-mass SMBHs as in NLS1 galaxies, and SMBH coalescences are the most efficient known mechanism to change SMBH spin on human timescales. However, there is no evidence based on the DESI host galaxy image that SDSS J1105+1452 has undergone a recent merger. The extended structures visible in the image are just the outer extension of the inner spiral arms rather than tidal tails. Without any further positive evidence of an ongoing or past merger, we do not discuss this rare scenario any further.

7.6.4. TDE

With the X-ray discovery of the first TDEs, a dedicated search for associated radio (jet) emission (S. Komossa & M. Dahlem 2001; S. Komossa 2002) was carried out. More sensitive recent radio observations have provided a high detection fraction of TDEs. The radio emission of the known TDEs, interpreted as jets and/or outflows, typically peaked $\sim 1-3$ yr after the optical or X-ray event, and then declined (A. Anumarlapudi et al. 2024; Y. Cendes et al. 2024). This is markedly different from SDSS J1105+1452, which remains radio bright and at roughly constant emission level for at least 8 yr implying a long-lasting constant power input. Slow circularization of the stellar debris (T. Piran et al. 2015; D. Lin et al. 2022) and/or rare disruption events of giant stars (J. Guillochon & E. Ramirez-Ruiz 2015; A. C. S. Readhead et al. 2024) might provide the required long-lasting near-constant power input but they have not yet been detected and further explored in the radio regime, and SDSS J1105+1452 would represent the first such case. The longer the radio outburst lasts at constant emission levels, the more challenging it will be to understand the outburst within this framework. Given the rarity of (giant) star disruptions and given the fact that SDSS J1105+1452 was already a (radio-)AGN before the outburst, we do not favor a TDE interpretation. We cannot entirely rule it out either, and will re-evaluate this scenario as our radio monitoring continues.

7.6.5. Activation of AGN Activity for the First Time

NLS1 galaxies are thought to be young AGN in an early stage of evolution (S. Mathur 2000; D. Grupe 2004). Therefore, is it conceivable that we may have witnessed the very first turn-on of accretion and AGN (jet) activity? This scenario can be rejected because the SDSS spectrum of 2005 already shows a classical NLR (traced by transitions like [Ne III]3798, [O III]5007, [O I]6300, and [S II]6716,31), implying AGN activity during at least the last thousands of years given light travel time constraints ($t_{\rm light} \sim$ 100s–1000s of years) and recombination timescale arguments ($t_{\rm rec} \sim$ 1000–10,000s of years). Further, the FIRST low-state radio emission implies a preexisting jet (Section 7.3).

7.6.6. Blazar Variability

Variability like that observed in blazars, due to Doppler boosting in a jet closely aligned with our LOS, was disfavored by GKK25. The variability pattern of SDSS J1105+1452 is very different from that of classical blazars that flare on timescales of days to months, but do not remain in a high state and at near-constant emission levels for years (H. D. Aller et al. 1985; C. M. Urry 1996; A. P. Marscher 2016). The steep optically thin part of the radio spectrum beyond a few GHz (Section 4, Figure 6) is different from blazars as well.

7.6.7. Change in Accretion Rate

In the last decade, a significant number of optical changing-look AGN have been identified. These are characterized by high-amplitude continuum and broad emission-line variability such that they change their optical spectroscopic Seyfert classification between type 1 and type 2 (or type 1.9, 1.8) and vice versa (review by S. Komossa et al. 2026). These changes occur on timescales of months to decades. Some systems turn on or off over years (K. D. Denney et al. 2014), others show fast changes within months and/or repeatedly transition between type 1 and type 2 (D. Alloin et al. 1986; L. Č. Popović et al. 2023; M. W. Ochmann et al. 2024). While the first changing-look events have been recognized in the 1960s–1980 s (Y. Andrillat & S. Souffrin 1968; D. Alloin et al. 1985; W. Kollatschny & K. J. Fricke 1985), larger numbers have been identified in recent years thanks to large-area optical sky surveys (P. J. Green et al. 2022; W.-J. Guo et al. 2024; Y.-H. Shen et al. 2025), and they have been detected not only in Seyfert galaxies but also in quasars (S. M. LaMassa et al. 2015; J. Wang et al. 2018; W.-J. Guo et al. 2025).

The high-amplitude continuum variability of changing-look AGN implies a change in accretion disk emission, but the physical drivers behind rapid changes in the accretion rate much faster than the viscous timescale have remained largely unknown, and a variety of different models have been explored in recent years (e.g., D. Grupe et al. 2015; D. Stern et al. 2018; M. Sniegowska et al. 2020; J. Wang et al. 2024; N. Kaaz et al. 2025; S.-L. Li & X. Cao 2025), including variants where magnetic fields play an important role (J. Dexter & M. C. Begelman 2019; N. Scepi et al. 2021; S. Laha et al. 2022; X. Cao et al. 2023; W.-B. Wu & W.-M. Gu 2023).

A few changing-look AGN with dedicated or archival radio follow-ups have shown clear changes in their radio emission (J. Y. Koay et al. 2016; S. Birmingham et al. 2025; A. Jana et al. 2025; E. T. Meyer et al. 2025). The majority of optical changing-look events have so far been identified in BLQ1s and BLS1s. In recent years, an intense search for similar optical events in NLS1 galaxies has been ongoing, and only a few cases have been identified so far (S. Frederick et al. 2019; W. J. Hon et al. 2022; S. Komossa & D. Grupe 2024; D. W. Xu et al. 2024; J. Wang et al. 2026). SDSS J1105+1452 is the first case that shows a long-lived radio changing-look.

We suggest that the radio turn-on event of SDSS J1105 +1452 was due to a change in accretion rate that triggered a dramatic increase in jet power and thus radio emission. The majority of recent accretion disk variability models (e.g., D. Stern et al. 2018; J. Dexter & M. C. Begelman 2019; M. Sniegowska et al. 2020; J. Wang et al. 2024; N. Kaaz et al. 2025; S.-L. Li & X. Cao 2025) do not yet provide immediate

predictions for the changes in radio jet emission and evolution. In particular, the amplitude of optical or X-ray variability (any increase or decrease) does not need to match the amplitude of radio variability (an observed factor of 23), and there can be a time delay between the optical/X-ray change and the increase in radio emission (see also footnote [28]).

As an example, we consider the following scenario. A way to reconcile a modest change in the accretion luminosity (e.g., a factor of at least 2 variability suggested by the low-cadence X-ray observations) with an extreme radio brightening (factor of $\sim$20) is to allow the jet efficiency to change nonlinearly, controlled by the net poloidal magnetic flux threading the SMBH, $\Phi_{\rm BH}$. In Blandford–Znajek-type jets, the jet power scales approximately as $P_{\rm jet} \propto \Phi_{\rm BH}^2 \Omega_{\rm H}^2$ (R. D. Blandford & R. L. Znajek 1977), and GRMHD simulations show that once the inner flow approaches the magnetically arrested disk (MAD) limit, the jet efficiency can increase dramatically at nearly fixed radiative output (R. Narayan et al. 2003; A. Tchekhovskoy et al. 2011; J. C. McKinney et al. 2012). Importantly, the mapping from jet power to centimeter-band radio luminosity is itself nonlinear; empirical X-ray-cavity–jet-power scalings imply $P_{\rm jet} \propto L_{\rm R}^{0.7-0.8}$ (K. W. Cavagnolo et al. 2010), so a 20-fold increase in radio luminosity corresponds to only a 6–9 fold increase in kinetic power. We emphasize that the cavity-power scaling is used here only to illustrate the nonlinear mapping between radio luminosity and jet power, not as a precise estimator of $P_{\rm jet}$ for this compact NLS1 galaxy. If $P_{\rm jet} \propto \Phi_{\rm BH}^2$ (at fixed BH spin), the required change in $\Phi_{\rm BH}$ is then only a factor of 2.4–3, i.e., a comparatively modest increase in net magnetic field flux can plausibly yield an order-of-magnitude radio transition without invoking an order-of-magnitude change in $\dot{M}$. Such flux growth can occur if the inner disk crosses from a diffusion-dominated to an advection-dominated flux-transport regime, because the inward advection of large-scale field competes with outward turbulent diffusion (S. H. Lubow et al. 1994). The rarity of such events in NLS1/BLS1 populations can be qualitatively understood if the supply of coherent net vertical flux (i.e., a sustained polarity imbalance) is itself intermittent: many accretion episodes may deliver mixed-polarity fields that cancel before reaching the black hole, whereas only a small subset of episodes advect sufficient net $\Phi_{\rm BH}$ to cross a MAD-like threshold and trigger a high-efficiency jet (see also T. An 2026). Recent VLBI observations of relativistic jet activity of the radio-quiet AGN Mrk 110 provide observational support for such episodic jet activation in a radio-quiet/NLS1-like system (A. Wang et al. 2025).

In summary, there is ample evidence for a coupling between disk and jet changes in classical AGN (A. P. Marscher et al. 2002) and Galactic binaries (R. Fender & T. Belloni 2004), and the violent and rapid changes in the structure and dynamics of magnetized disks in changing-look events are expected to directly fuel the launch of jets and outflows.

8. Summary and Conclusions

We have reported new and first observations across the electromagnetic spectrum of the recently discovered unique long-duration radio outburst of an NLS1 galaxy. Owing to its low redshift, a large number of archival and new MWL observations could be obtained that would have been missing at higher redshifts. The salient results on MWL properties and interpretation of the unprecedented radio changing-look event of SDSS J1105+1452 can be summarized as follows:

1. Different methods of SMBH mass determination provide a mass in the range of (2.8–4.4) $\times$ 10^6 $M_\odot$ and a high Eddington ratio of $\lambda_{\rm Edd} = 0.2-0.3$. These values corroborate the optical NLS1 classification.
2. The photon index of the first (0.3–10) keV X-ray spectrum of SDSS J1105+1452, $\Gamma_{\rm X} = 2.5$, shows that the spectrum is steep and consistent with a contribution from accretion disk emission.
3. The absorption and extinction along our LOS, measured from X-ray and optical observations, is low; $E(B-V) \leqslant 0.05-0.1$ (from the optical) and $N_{\rm H} \leqslant 3.1 \times 10^{20}$ cm^{-2} (from X-ray spectral fits). Therefore, along our LOS, significant amounts of dusty or dust-free absorbers are absent.
4. Several different arguments demonstrate that the star formation activity is moderate and the low-state radio emission is still dominated by the AGN.
5. The radio SED, measured for the first time beyond several GHz, declines steeply at high frequencies. The SED is low-frequency peaked. It is well fit by a phenomenological parabola in log-log space and turns over at 2.1 GHz. When described by a power law, the SED declines with a spectral index of $\alpha_{\rm thick} = 1.6 \pm 0.1$ toward low frequencies. At 4.85 GHz, $L_{4.85\ \rm GHz} = 7 \times 10^{40}$ erg s^{-1}.
6. Radio observations between 2017 December and 2026 January show that the radio outburst is remarkably long-lived. It has lasted at least 8 yr at roughly constant flux density.
7. Inspection of archival optical/IR data reveals no systematic high-amplitude change since 2003. Therefore, if the radio turn-on was accompanied by a significant optical/IR change, the trigger likely occurred before 2003. This includes the possibility that an earlier disk change, as traced by, e.g., the higher X-ray state observed during the RASS, or the high blue magnitude during POSS, triggered the jet launch but a significant rise in radio emission only occurred several years later.
8. A variety of different outburst scenarios were considered, including lensing, variants of absorption variability, the presence of a binary SMBH or a coalescence-driven spin flip, a TDE, AGN ignition for the first time, and accretion disk variability as in optical changing-look events. The majority of them can either be rejected or are deemed too rare (an SMBH spin flip following binary coalescence, or a giant-star TDE) to warrant further exploration at this stage in the absence of supporting evidence. However, in the era of SKA with ongoing and upcoming deep large-area sky surveys, we expect that all of these transient phenomena and physics will be discovered and explored at some stage. We suggest that a change in the accretion rate, as observed for instance in optical changing-look AGN, powered a long-lived change, a strong increase, in the radio jet emission of SDSS J1105+1452.

Multiple follow-up observations are ongoing and/or are of interest. Ongoing radio monitoring will follow the evolution of the radio jet and enable a search for any turn-off. This then

offers an excellent chance to trace radio (and MWL) turn-off physics. SDSS J1105+1452 may even undergo recurrent radio changing-look transitions, as observed in the optical regime in a fraction of the optical changing-look events in broad-line type 1 AGN (e.g., S. Panda & M. Śniegowska 2024; J. Wang et al. 2024; Q. Dong et al. 2025). High-resolution VLBI imaging will determine the location and compactness of the jet down to parsec scales. HI 21 cm absorption spectroscopy at the redshift of SDSS J1105+1452 will provide the amount of cold hydrogen absorption directly along our LOS toward the radio source. New optical spectroscopy will allow us to search for evolution in the emission lines. Deep XMM-Newton X-ray spectroscopy will disentangle the soft excess and power-law (jet and corona) emission. SDSS J1105+1452, despite its excellent coverage, still suffered from gaps in MWL data. A dedicated search for new, similar transient events in their rise phase in currently ongoing radio surveys will have the benefit of available simultaneous dense coverage in optical surveys, including the Large Synoptic Survey Telescope (Ž. Ivezić et al. 2019).

While the majority of NLS1 galaxies are constant radio emitters, the case of SDSS J1105+1452 highlights that some can undergo decade-long dramatic radio changing-look transitions between radio-quiet and radio-loud, and SDSS J1105+1452 may be the prototype of a new time-domain radio AGN class. Establishing the physics behind new types of long-lived radio transients provides us with important new insights into the mechanisms of radio jet formation and evolution under extreme conditions and their impact on the ISM, and sets the stage for the future search for such transients in the era of SKA.

Acknowledgments

We would like to thank the Swift team for carrying out the observations we proposed. It is our pleasure to thank Krzysztof Stanek for many very helpful discussions about the ASAS-SN data and Emil Lenc for very useful discussions. We would like to thank our referee for many useful suggestions. S.K. would like to thank the CAS President's International Fellowship Initiative for partial support. S.K. and R.S. would like to thank NAOC Beijing for their hospitality. S.K. would also like to thank Shanghai Observatory for its hospitality. M.J.H. thanks the UK STFC for support [ST/Y001249/1]. K.É.G. was supported by HUN-REN, and the NKFIH excellence grant TKP2021-NKTA-64. S.P. is supported by the international Gemini Observatory, a program of NSF NOIRLab, which is managed by the Association of Universities for Research in Astronomy (AURA) under a cooperative agreement with the U.S. National Science Foundation, on behalf of the Gemini partnership of Argentina, Brazil, Canada, Chile, the Republic of Korea, and the United States of America. D.W.X. is supported by the National Natural Science Foundation of China under grant No. 12273054. This work is partly based on data obtained with the 100 m telescope of the Max-Planck-Institut für Radioastronomie at Effelsberg. The Australia Telescope Compact Array is part of the Australia Telescope National Facility (https://ror.org/05qajvd42), which is funded by the Australian Government for operation as a National Facility managed by CSIRO. We acknowledge the Gomeroi people as the Traditional Owners of the Observatory site. This work uses data obtained from Inyarrimanha Ilgari Bundara/the CSIRO's Murchison Radio-astronomy Observatory. We acknowledge the Wajarri Yamaji People as the Traditional Owners and native title holders of the Observatory site. CSIRO's ASKAP radio telescope is part of the Australia Telescope National Facility (https://ror.org/05qajvd42). Operation of ASKAP is funded by the Australian Government with support from the National Collaborative Research Infrastructure Strategy. ASKAP uses the resources of the Pawsey Supercomputing Research Centre. Establishment of ASKAP, Inyarrimanha Ilgari Bundara, the CSIRO Murchison Radio-astronomy Observatory, and the Pawsey Supercomputing Research Centre are initiatives of the Australian Government, with support from the Government of Western Australia and the Science and Industry Endowment Fund. LOFAR is the Low Frequency Array designed and constructed by ASTRON. It has observing, data processing, and data storage facilities in several countries, which are owned by various parties (each with its own funding sources), and which are collectively operated by the LOFAR ERIC under a joint scientific policy. The LOFAR resources have benefited from the following recent major funding sources: CNRS-INSU, Observatoire de Paris and Université d'Orléans, France; BMBF, MIWF-NRW, MPG, Germany; Science Foundation Ireland (SFI), Department of Business, Enterprise and Innovation (DBEI), Ireland; NWO, The Netherlands; The Science and Technology Facilities Council, UK; Ministry of Science and Higher Education, Poland; The Istituto Nazionale di Astrofisica (INAF), Italy. This research made use of the Dutch national e-infrastructure with support of the SURF Cooperative (e-infra 180169) and the LOFAR e-infra group. The Jülich LOFAR Long Term Archive and the German LOFAR network are both coordinated and operated by the Jülich Supercomputing Centre (JSC), and computing resources on the supercomputer JUWELS at JSC were provided by the Gauss Centre for Supercomputing e.V. (grant CHTB00) through the John von Neumann Institute for Computing (NIC). This research made use of the University of Hertfordshire high-performance computing facility and the LOFAR-UK computing facility located at the University of Hertfordshire and supported by STFC [ST/P000096/1], and of the Italian LOFAR IT computing infrastructure supported and operated by INAF, and by the Physics Department of Turin University (under an agreement with Consorzio Interuniversitario per la Fisica Spaziale) at the C3S Supercomputing Centre, Italy. This research is part of the project LOFAR Data Valorization (LDV) [project numbers 2020.031, 2022.033, and 2024.047] of the research program Computing Time on National Computer Facilities using SPIDER that is (co-)funded by the Dutch Research Council (NWO), hosted by SURF through the call for proposals of Computing Time on National Computer Facilities. This research has made use of the NASA/IPAC Extragalactic Database (NED), which is operated by the Jet Propulsion Laboratory, California Institute of Technology, under contract with the National Aeronautics and Space Administration. This research has made use of NASA's Astrophysics Data System (ADS) Bibliographic Services.

Facilities: Neil Gehrels Swift Observatory (XRT and UVOT), Effelsberg 100 m telescope, ATCA, ASKAP, and LOFAR.

Software: `HEASoft` (https://heasarc.gsfc.nasa.gov/docs/software/heasoft/) with `XSPEC` (K. A. Arnaud 1996), `ESO-MIDAS` (https://www.eso.org/sci/software/esomidas/), XRT Data Analysis Software (`XRTDAS`) developed under

the responsibility of the ASI Science Data Center (ASDC), Italy (https://www.ssdc.asi.it/), `RadioSED` (E. F. Kerrison et al. 2024, https://github.com/ekerrison/RadioSED), `CASA` (CASA Team et al. 2022), and `Miriad` (R. J. Sault et al. 1995).

Data Availability

The Swift data of our project are available in the Swift archive at https://swift.gsfc.nasa.gov/archive/. Effelsberg and ATCA data are available upon reasonable request. Archived ASKAP data can be obtained through the CSIRO ASKAP Science Data Archive, CASDA, at http://data.csiro.au/.

ORCID iDs

S. Komossa https://orcid.org/0000-0003-4183-4215
D. Grupe https://orcid.org/0000-0002-9961-3661
A. Kraus https://orcid.org/0000-0002-4184-9372
P.G. Edwards https://orcid.org/0000-0002-8186-4753
E. F. Kerrison https://orcid.org/0000-0002-0011-6922
K. Rose https://orcid.org/0000-0002-7329-3209
R. Soria https://orcid.org/0000-0002-4622-796X
T. An https://orcid.org/0000-0003-4341-0029
M.J. Hardcastle https://orcid.org/0000-0003-4223-1117
K.É. Gabányi https://orcid.org/0000-0003-1020-1597
S. Panda https://orcid.org/0000-0002-5854-7426
D.W. Xu https://orcid.org/0000-0002-7475-7247
J. Wang https://orcid.org/0000-0002-6880-4481
S. Frey https://orcid.org/0000-0003-3079-1889
A. Mezősi https://orcid.org/0009-0004-6695-5122

References

Adelman-McCarthy, J. K., Abazajian, K. N., Agüeros, M. A., et al. 2009, yCat, 2294
Aller, H. D., Aller, M. F., Latimer, G. E., & Hodge, P. E. 1985, ApJS, 59, 513
Alloin, D., Pelat, D., Phillips, M., & Whittle, M. 1985, ApJ, 288, 205
Alloin, D., Pelat, D., Phillips, M. M., Fosbury, R. A. E., & Freeman, K. 1986, ApJ, 308, 23
An, T. 2026, arXiv:2603.21119
Anderson, S. F., Margon, B., Voges, W., et al. 2007, AJ, 133, 313
Andrillat, Y., & Souffrin, S. 1968, ApL, 1, 111
Angelakis, E., Fuhrmann, L., Marchili, N., et al. 2015, A&A, 575, A55
Anumarlapudi, A., Dobie, D., Kaplan, D. L., et al. 2024, ApJ, 974, 241
Arnaud, K. A. 1996, ASPC, 101, 17
Barrows, R. S., Comerford, J. M., Stern, D., & Assef, R. J. 2021, ApJ, 922, 179
Bellm, E. C., Kulkarni, S. R., Graham, M. J., et al. 2019, PASP, 131, 018002
Bicknell, G. V., Mukherjee, D., Wagner, A. Y., Sutherland, R. S., & Nesvadba, N. P. H. 2018, MNRAS, 475, 3493
Bietenholz, M. F., Bartel, N., Argo, M., et al. 2021, ApJ, 908, 75
Birmingham, S., Ward, C., Nyland, K., et al. 2025, arXiv:2507.01355
Blandford, R. D., & Znajek, R. L. 1977, MNRAS, 179, 433
Bloom, J. S., Giannios, D., Metzger, B. D., et al. 2011, Sci, 333, 203
Boroson, T. A. 2002, ApJ, 565, 78
Breeveld, A. A., Curran, P. A., Hoversten, E. A., et al. 2010, MNRAS, 406, 1687
Burrows, D. N., Hill, J. E., Nousek, J. A., et al. 2005, SSRv, 120, 165
Campanelli, M., Lousto, C., Zlochower, Y., & Merritt, D. 2007, ApJL, 659, L5
Cao, X., You, B., & Wei, X. 2023, MNRAS, 526, 2331
Cardelli, J. A., Clayton, G. C., & Mathis, J. S. 1989, ApJ, 345, 245
CASA Team, Bean, B., Bhatnagar, S., et al. 2022, PASP, 134, 114501
Cash, W. 1979, ApJ, 228, 939
Cavagnolo, K. W., McNamara, B. R., Nulsen, P. E. J., et al. 2010, ApJ, 720, 1066
Cendes, Y., Berger, E., Alexander, K. D., et al. 2024, ApJ, 971, 185
Chen, S., Stevens, J. B., Edwards, P. G., et al. 2022, MNRAS, 512, 471
Chen, Y., Gaensler, B. M., Clarke, T., et al. 2025, ApJ, 987, 170
Condon, J. J., Cotton, W. D., Greisen, E. W., et al. 1998, AJ, 115, 1693
Dalla Bontà, E., Peterson, B. M., Grier, C. J., et al. 2025, A&A, 696, A48
de Vries, W. H., O'Dea, C. P., Barthel, P. D., et al. 2000, AJ, 120, 2300
Denney, K. D., De Rosa, G., Croxall, K., et al. 2014, ApJ, 796, 134
Dexter, J., & Begelman, M. C. 2019, MNRAS, 483, L17
Dey, A., Schlegel, D. J., Lang, D., et al. 2019, AJ, 157, 168
Dong, Q., Zhang, Z.-X., Gu, W.-M., et al. 2025, arXiv:2510.18445
D'Orazio, D. J., Haiman, Z., & MacFadyen, A. 2013, MNRAS, 436, 2997
Drake, A. J., Djorgovski, S. G., Mahabal, A., et al. 2009, ApJ, 696, 870
Duchesne, S., Ross, K., Thomson, A. J. M., et al. 2025, PASA, 42, 38
Duchesne, S. W., Grundy, J. A., Heald, G. H., et al. 2024, PASA, 41, e003
Elvis, M., Wilkes, B. J., McDowell, J. C., et al. 1994, ApJS, 95, 1
Evans, P. A., Beardmore, A. P., Page, K. L., et al. 2007, A&A, 469, 379
Fender, R., & Belloni, T. 2004, ARA&A, 42, 317
Ferguson, J. W., Korista, K. T., & Ferland, G. J. 1997, ApJS, 110, 287
Frail, D. A., Kulkarni, S. R., Nicastro, L., Feroci, M., & Taylor, G. B. 1997, Natur, 389, 261
Frederick, S., Gezari, S., Graham, M. J., et al. 2019, ApJ, 883, 31
Gabányi, K. É., Komossa, S., Kraus, A., MezÅŚsi, A., & Frey, S. 2025, A&A, 702, L17
Gaia Collaboration, Vallenari, A., Brown, A. G. A., et al. 2023, A&A, 674, A1
Gaskell, C. M. 2017, MNRAS, 467, 226
Gavras, P., Rimoldini, L., Nienartowicz, K., et al. 2023, A&A, 674, A22
Gehrels, N., Chincarini, G., Giommi, P., et al. 2004, ApJ, 611, 1005
Goodrich, R. W. 1989, ApJ, 342, 224
Gordon, Y. A., Boyce, M. M., O'Dea, C. P., et al. 2021, ApJS, 255, 30
Green, P. J., Pulgarin-Duque, L., Anderson, S. F., et al. 2022, ApJ, 933, 180
Gregory, P. C., Scott, W. K., Douglas, K., & Condon, J. J. 1996, ApJS, 103, 427
Grupe, D. 2004, AJ, 127, 1799
Grupe, D., Komossa, S., Leighly, K. M., & Page, K. L. 2010, ApJS, 187, 64
Grupe, D., Komossa, S., & Saxton, R. 2015, ApJL, 803, L28
Guillochon, J., & Ramirez-Ruiz, E. 2015, ApJ, 809, 166
Gültekin, K., Richstone, D. O., Gebhardt, K., et al. 2009, ApJ, 698, 198
Guo, W.-J., Pan, Z., Siudek, M., et al. 2025, ApJL, 981, L8
Guo, W.-J., Zou, H., Fawcett, V. A., et al. 2024, ApJS, 270, 26
Hale, C. L., McConnell, D., Thomson, A. J. M., et al. 2021, PASA, 38, e058
Hancock, P. J., Charlton, E. G., Macquart, J.-P., & Hurley-Walker, N. 2019, arXiv:1907.08395
Hancock, P. J., Gaensler, B. M., & Murphy, T. 2013, ApJ, 776, 106
Helfand, D. J., White, R. L., & Becker, R. H. 2015, ApJ, 801, 26
HI4PI Collaboration, Ben Bekhti, N., Flöer, L., et al. 2016, A&A, 594, A116
Hill, J. E., Burrows, D. N., Nousek, J. A., et al. 2004, SPIE, 5165, 217
Hon, W. J., Wolf, C., Onken, C. A., Webster, R., & Auchettl, K. 2022, MNRAS, 511, 54
Hopkins, A. M., Miller, C. J., Nichol, R. C., et al. 2003, ApJ, 599, 971
Hurley-Walker, N., Callingham, J. R., Hancock, P. J., et al. 2017, MNRAS, 464, 1146
Huynh, M., Dempsey, J., Whiting, M. T., & Ophel, M. 2020, ASPC, 522, 263
Ivezić, Ž., Kahn, S. M., Tyson, J. A., et al. 2019, ApJ, 873, 111
Jana, A., Ricci, C., Venselaar, S. M., et al. 2025, A&A, 699, A62
Jarrett, T. H., Cohen, M., Masci, F., et al. 2011, ApJ, 735, 112
Järvelä, E., Savolainen, T., Berton, M., et al. 2024, MNRAS, 532, 3069
Kaaz, N., Liska, M., Ward, C., & Davelaar, J. 2025, arXiv:2511.09626
Kellermann, K. I., Sramek, R., Schmidt, M., Shaffer, D. B., & Green, R. 1989, AJ, 98, 1195
Kerrison, E. F., Allison, J. R., Moss, V. A., Sadler, E. M., & Rees, G. A. 2024, MNRAS, 533, 4248
Koay, J. Y., Vestergaard, M., Bignall, H. E., Reynolds, C., & Peterson, B. M. 2016, MNRAS, 460, 304
Kochanek, C. S., Shappee, B. J., Stanek, K. Z., et al. 2017, PASP, 129, 104502
Kollatschny, W., & Fricke, K. J. 1985, A&A, 146, L11
Komossa, S. 2002, RvMA, 15, 27
Komossa, S. 2008, RMxAC, 32, 86
Komossa, S. 2018, in Proc. Sci., Revisiting Narrow-Line Seyfert 1 Galaxies and Their Place in the Universe (NLS1-2018), Vol. 328, (SISSA), 15
Komossa, S., & Dahlem, M. 2001, arXiv:astro-ph/0106422
Komossa, S., & Grupe, D. 2024, SerAJ, 209, 1
Komossa, S., Voges, W., Xu, D., et al. 2006, AJ, 132, 531
Komossa, S., Kraus, A., Grupe, D., et al. 2023, ApJ, 944, 177
Komossa, S., Grupe, D., Marziani, P., et al. 2026, AdSpR, 77, 4041
Kraus, A., Krichbaum, T. P., Wegner, R., et al. 2003, A&A, 401, 161
Kunert-Bajraszewska, M., Janiuk, A., Siemiginowska, A., & Gawroński, M. 2011, IAUS, 275, 180
Kunert-Bajraszewska, M., Kozieł-Wierzbowska, D., Stern, D., et al. 2025, A&A, 704, A3
Kunert-Bajraszewska, M., Wołowska, A., Mooley, K., Kharb, P., & Hallinan, G. 2020, ApJ, 897, 128

Lacy, M., Baum, S. A., Chandler, C. J., et al. 2020, PASP, 132, 035001
Laha, S., Meyer, E., Roychowdhury, A., et al. 2022, ApJ, 931, 5
LaMassa, S. M., Cales, S., Moran, E. C., et al. 2015, ApJ, 800, 144
Li, D., Zhang, W., Yang, J., et al. 2025, SciBu, 71, 538
Li, S.-L., & Cao, X. 2025, ApJ, 988, 207
Lin, D., Godet, O., Webb, N. A., et al. 2022, ApJL, 924, L35
Lister, M. 2018, Proc. Sci. Revisiting Narrow-Line Seyfert 1 Galaxies and Their Place in the Universe, POS(NLS1-2018), Vol. 328 (SISSA), 22
Lubow, S. H., Papaloizou, J. C. B., & Pringle, J. E. 1994, MNRAS, 268, 1010
Mainzer, A., Bauer, J., Cutri, R. M., et al. 2014, ApJ, 792, 30
Maiolino, R., Scholtz, J., Witstok, J., et al. 2024, Natur, 627, 59
Marscher, A. P. 2016, Galax, 4, 37
Marscher, A. P., Jorstad, S. G., Gómez, J.-L., et al. 2002, Natur, 417, 625
Marziani, P., Dultzin, D., Sulentic, J. W., et al. 2018, FrASS, 5, 6
Masci, F. J., Laher, R. R., Rusholme, B., et al. 2019, PASP, 131, 018003
Mathur, S. 2000, MNRAS, 314, L17
Matt, G., Guainazzi, M., & Maiolino, R. 2003, MNRAS, 342, 422
McConnell, D., Hale, C. L., Lenc, E., et al. 2020, PASA, 37, e048
McKinney, J. C., Tchekhovskoy, A., & Blandford, R. D. 2012, MNRAS, 423, 3083
Meyer, E. T., Laha, S., Shuvo, O. I., et al. 2025, ApJL, 979, L2
Mezger, P. G., & Henderson, A. P. 1967, ApJ, 147, 471
Milosavljević, M., & Phinney, E. S. 2005, ApJL, 622, L93
Monet, D. G., Levine, S. E., Canzian, B., et al. 2003, AJ, 125, 984
Narayan, R., Igumenshchev, I. V., & Abramowicz, M. A. 2003, PASJ, 55, L69
Netzer, H. 2013, The Physics and Evolution of Active Galactic Nuclei (Cambridge Univ. Press)
Nyland, K., Dong, D. Z., Patil, P., et al. 2020, ApJ, 905, 74
Ochmann, M. W., Kollatschny, W., Probst, M. A., et al. 2024, A&A, 686, A17
O'Dea, C. P. 1998, PASP, 110, 493
O'Dea, C. P., & Baum, S. A. 1997, AJ, 113, 148
O'Dea, C. P., & Saikia, D. J. 2021, A&ARv, 29, 3
Oh, K., Yi, S. K., Schawinski, K., et al. 2015, ApJS, 219, 1
Osterbrock, D. E. 1989, (University Science Books, Mill Valley)
Osterbrock, D. E., & Pogge, R. W. 1985, ApJ, 297, 166
Paliya, V. S., Stalin, C. S., Domínguez, A., & Saikia, D. J. 2024, MNRAS, 527, 7055
Panda, S. 2021, A&A, 650, A154
Panda, S., & Śniegowska, M. 2024, ApJS, 272, 13
Park, T., Kashyap, V. L., Siemiginowska, A., et al. 2006, ApJ, 652, 610
Piran, T., Sadowski, A., & Tchekhovskoy, A. 2015, MNRAS, 453, 157
Poole, T. S., Breeveld, A. A., Page, M. J., et al. 2008, MNRAS, 383, 627
Popović, L. Č., Ilić, D., Burenkov, A., et al. 2023, A&A, 675, A178
Predehl, P., & Schmitt, J. H. M. M. 1995, A&A, 293, 889
Puchnarewicz, E. M., Mason, K. O., Cordova, F. A., et al. 1992, MNRAS, 256, 589
Rakshit, S., Stalin, C. S., Chand, H., & Zhang, X.-G. 2017, ApJS, 229, 39
Readhead, A. C. S., Ravi, V., Blandford, R. D., et al. 2024, ApJ, 961, 242
Reynolds, C. S., & Begelman, M. C. 1997, ApJL, 487, L135
Roming, P. W. A., Kennedy, T. E., Mason, K. O., et al. 2005, SSRv, 120, 95
Rose, K., Horesh, A., Murphy, T., et al. 2024, MNRAS, 534, 3853
Sault, R. J., Teuben, P. J., & Wright, M. C. H. 1995, ASPC, 77, 433
Scepi, N., Begelman, M. C., & Dexter, J. 2021, MNRAS, 502, L50
Schlegel, E. M. 1990, MNRAS, 244, 269
Shao, X., Edwards, P. G., Stevens, J., et al. 2025, MNRAS, 536, 1344
Shappee, B. J., Prieto, J. L., Grupe, D., et al. 2014, ApJ, 788, 48
Shen, Y.-H., Lu, K.-X., Guo, W.-J., et al. 2025, ApJ, 994, 203
Shimwell, T. W., Hardcastle, M. J., Tasse, C., et al. 2026, A&A, 707, A198
Sniegowska, M., Czerny, B., Bon, E., & Bon, N. 2020, A&A, 641, A167
Stern, D., McKernan, B., Graham, M. J., et al. 2018, ApJ, 864, 27
Sukumar, S., & Allen, R. J. 1989, ApJ, 341, 883
Sulentic, J. W., Marziani, P., & Dultzin-Hacyan, D. 2000, ARA&A, 38, 521
Sun, J., & Shen, Y. 2015, ApJL, 804, L15
Tchekhovskoy, A., Narayan, R., & McKinney, J. C. 2011, MNRAS, 418, L79
Terashima, Y., & Wilson, A. S. 2003, ApJ, 583, 145
Truemper, J. 1982, AdSR, 2, 241
Urry, C. M. 1996, ASPC, 110, 391
Varglund, I., Järvelä, E., Hardcastle, M. J., Varglund, S., & Lähteenmäki, A. 2025, A&A, 703, A202
Véron-Cetty, M. P., Véron, P., & Gonçalves, A. C. 2001, A&A, 372, 730
Vestergaard, M., & Peterson, B. M. 2006, ApJ, 641, 689
Viswanath, G., Stalin, C. S., Rakshit, S., et al. 2019, ApJL, 881, L24
Voges, W., Aschenbach, B., Boller, T., et al. 1999, A&A, 349, 389
Wang, A., An, T., Kellermann, K. I., et al. 2025, ApJL, 987, L26
Wang, J., Xu, D. W., Cao, X., et al. 2024, ApJ, 970, 85
Wang, J., Jin, S., Xu, D. W., et al. 2026, ApJ, 1002, 85
Wang, J., Xu, D. W., & Wei, J. Y. 2018, ApJ, 858, 49
White, R. L., Becker, R. H., Helfand, D. J., & Gregg, M. D. 1997, ApJ, 475, 479
Whiting, M., & Humphreys, B. 2012, PASA, 29, 371
Wilms, J., Allen, A., & McCray, R. 2000, ApJ, 542, 914
Wołowska, A., Kunert-Bajraszewska, M., Mooley, K. P., et al. 2021, ApJ, 914, 22
Wright, E. L. 2006, PASP, 118, 1711
Wright, E. L., Eisenhardt, P. R. M., Mainzer, A. K., et al. 2010, AJ, 140, 1868
Wu, W.-B., & Gu, W.-M. 2023, ApJ, 958, 146
Xu, D., Komossa, S., Zhou, H., et al. 2012, AJ, 143, 83
Xu, D. W., Komossa, S., Grupe, D., et al. 2024, Univ, 10, 61
Yoon, H., Sadler, E. M., Mahony, E. K., et al. 2025, PASA, 42, e088
York, D. G., Adelman, J., Anderson, John, E. J., et al. 2000, AJ, 120, 1579
Yuan, W., Zhou, H. Y., Komossa, S., et al. 2008, ApJ, 685, 801
Zhang, F., Shu, X., Sun, L., et al. 2022, ApJ, 938, 43
Zhou, H., Wang, T., Yuan, W., et al. 2007, ApJL, 658, L13